Stem Cell Reports
Article

ISSCR

OPEN ACCESS

Altered patterning of trisomy 21 interneuron progenitors

Yathindar Giffin-Rao,[1] Jie Sheng,[1,4] Bennett Strand,[1] Ke Xu,[1] Leslie Huang,[1] Margaret Medo,[1] Kirstin A. Risgaard,[1] Samuel Dantinne,[1] Sruti Mohan,[1] Aratrika Keshan,[1] Roger A. Daley, Jr.,[1] Bradley Levesque,[1] Lindsey Amundson,[1] Rebecca Reese,[1] André M.M. Sousa,[1,3] Yunlong Tao,[1] Daifeng Wang,[1,4] Su-Chun Zhang,[1,3,5] and Anita Bhattacharyya[1,2,*]

[1]Waisman Center, University of Wisconsin-Madison, Madison, WI 53705, USA
[2]Department of Cell and Regenerative Biology, School of Medicine and Public Health, University of Wisconsin-Madison, Madison, WI 53705, USA
[3]Department of Neuroscience, School of Medicine and Public Health, University of Wisconsin-Madison, Madison, WI 53705, USA
[4]Department of Biostatistics and Medical Informatics, School of Medicine and Public Health, University of Wisconsin-Madison, Madison, WI 53705, USA
[5]Department of Neurology, School of Medicine and Public Health, University of Wisconsin-Madison, Madison, WI 53705, USA
*Correspondence: bhattacharyy@waisman.wisc.edu
https://doi.org/10.1016/j.stemcr.2022.05.001

SUMMARY

Individuals with Down syndrome (DS; Ts21), the most common genetic cause of intellectual disability, have smaller brains that reflect fewer neurons at pre- and post-natal stages, implicating impaired neurogenesis during development. Our stereological analysis of adult DS cortex indicates a reduction of calretinin-expressing interneurons. Using Ts21 human induced pluripotent stem cells (iPSCs) and isogenic controls, we find that Ts21 progenitors generate fewer COUP-TFII+ progenitors with reduced proliferation. Single-cell RNA sequencing of Ts21 progenitors confirms the altered specification of progenitor subpopulations and identifies reduced WNT signaling. Activation of WNT signaling partially restores the COUP-TFII+ progenitor population in Ts21, suggesting that altered WNT signaling contributes to the defective development of cortical interneurons in DS.

INTRODUCTION

The human cortex has evolved larger superficial layers and greater reliance on interneurons for complex functions than other mammals (Arshad et al., 2016; Dzaja et al., 2014; Hansen et al., 2013; Jones, 2009; Paredes et al., 2016; Radonjic et al., 2014). Defects in cortical interneuron development and function are linked to many neuropsychiatric disorders and disorders characterized by intellectual disability (Marin, 2012; Rossignol, 2011). Maldevelopment can lead to abnormal numbers, subtypes, and/or placement of interneurons that significantly affect the functioning of the cortex, leading to cognitive impairment. The most common of these is Down syndrome (DS; trisomy 21 [Ts21]), a complex multigene disorder caused by Ts21.

DS individuals have smaller brains (Becker et al., 1991; Davidoff, 1928; Schmidt-Sidor et al., 1990; Wisniewski, 1990) with reduced volume of frontal and temporal areas of the cortex, including the hippocampus (Emerson et al., 1995; Kesslak et al., 1994; Wisniewski, 1990). Morphological analysis of pre- and post-natal DS brains over the last century has consistently revealed fewer neurons in DS brains (Becker et al., 1991; Benda, 1947; Colon, 1972; Davidoff, 1928; Golden and Hyman, 1994; Ross et al., 1984; Takashima et al., 1981; Wisniewski et al., 1984), underlying the reduced volume and implicating reduced neurogenesis as a feature in DS (Lott and Dierssen, 2010). In particular, fewer granular cells and aspinous stellate interneurons are present in upper cortical layers in early life (Ross et al., 1984). These neuropathological studies were based on small sample sizes and morphological identification of interneurons. Our own *in vitro* data on DS fetal tissue corroborates that neuron reductions include GABAergic neurons (Bhattacharyya et al., 2009). We and others have modeled interneuron development using Ts21 induced pluripotent stem cells (iPSCs) and found that generation of interneurons from Ts21 iPSCs is altered, both *in vitro* and when transplanted *in vivo* (Huo et al., 2018; Xu et al., 2019). These observations point to the simple fact that the development of cortical interneurons is impaired in DS. The processes underlying the maldevelopment of cortical interneurons in DS remain unknown.

We address gaps in knowledge of interneuron development in DS through rigorous analysis of post-mortem tissue to assess specific interneuron subpopulations for deficits and then model interneuron deficits using iPSCs from individuals with DS and isogenic controls to reveal if and how the initial events of specification and proliferation of cortical interneurons are altered in DS. Our results show specific deficits in calretinin (CR+) interneurons and altered specification and proliferation of progenitors at the cellular level. Molecular data suggest that reduced WNT signaling may be one of the mechanisms of faulty human interneuron development in DS.

RESULTS

Fewer interneurons in DS cortex

Limited histopathological observations reveal the presence of fewer neurons, primarily in superficial layers, in the DS

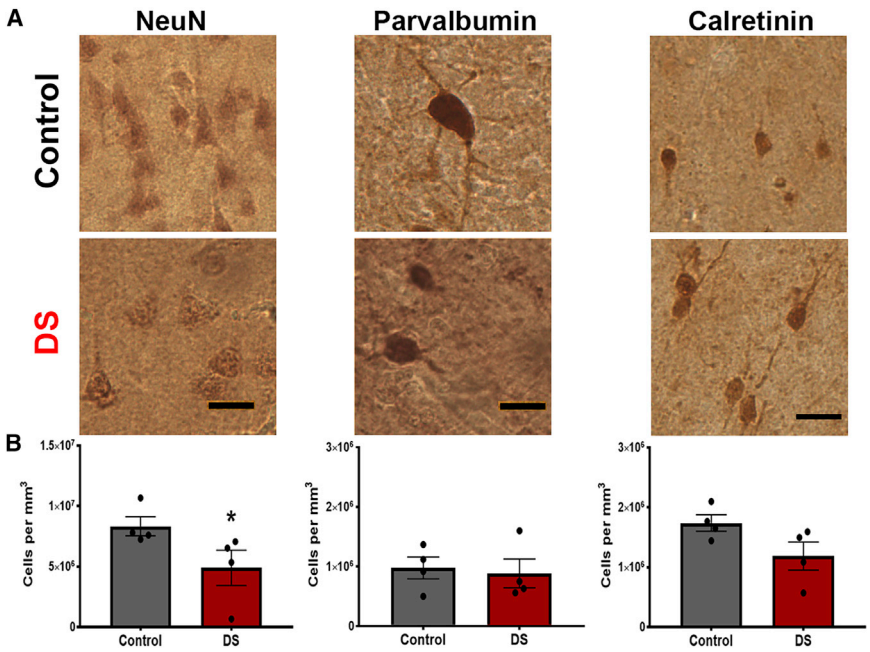

Figure 1. Reduced density of neurons in post-mortem Down syndrome cortex

(A) Representative images of NeuN+, PV+, and CR+ neurons detected by immunohistochemistry (DAB) in control and DS post-mortem superior temporal gyrus (STG) samples.

(B) Stereological quantification of the density of each neuron subtype in control and Down syndrome (DS) tissue. N = 4; NeuN *p = 0.03, PV p = 0.89, CR p = 0.11 calculated using non-parametric Mann-Whitney U test.

cortex (Golden and Hyman, 1994; Ross et al., 1984; Weitzdoerfer et al., 2001). Based on morphology, results suggest fewer aspinous stellate interneurons (Ross et al., 1984). We sought to determine whether there is a reduction in interneurons and, if so, to define which interneuron subtypes are altered, using immunohistochemical markers in DS cortex. We analyzed post-mortem superior temporal gyrus (STG) from four individuals with DS and four age-matched control male individuals (ages 15–35) (Figure 1A; supplemental experimental procedures). These adolescent and young-adult ages are similar to those in the previous study (Ross et al., 1984) and were chosen to avoid the early onset degeneration that occurs in individuals with DS as early as age 30 (Hartley et al., 2014). We analyzed the STG for several reasons: (1) thin STG is a consistent gross abnormality in DS brain (Becker, 1991; Mito et al., 1991), (2) alterations in neuron density and lamination in the STG occur during DS cortical development (Golden and Hyman, 1994), and (3) the STG is an association cortex likely to be involved in intellectual impairment in DS. Immunocytochemistry and design-based stereology were used to quantify neuronal populations in sections (Perl et al., 2000; West, 2013) to ensure unbiased, efficient, and more reliable results than other *ad hoc* quantitative analyses (Boyce et al., 2010) and to take into account the gross size differences of DS brains. We used the optical-fractionator-probe method (Stereo Investigator, MBF) to uniformly sample and estimate cell number and the Cavalieri-probe method to estimate volume (West et al., 1991). Our results show a reduced density of NeuN+ cells, corroborating the reduction in the number of neurons in DS cortex (Figure 1B; control = $8.33 \times 10^6 \pm 0.79 \times 10^6$, DS = $4.90 \times 10^6 \pm 0.15 \times 10^6$, p = 0.029, N = 4). Using parvalbumin (PV) to identify the predominant interneuron subtype in mouse, we observed no density difference in this population between DS and controls (control = $0.98 \times 10^6 \pm 0.18 \times 10^6$, DS = $0.89 \times 10^6 \pm 0.24 \times 10^6$, p = 0.89, N = 4). Using CR as a marker of upper-layer interneurons, we find a greater proportion of CR+ neurons than PV+ neurons in both control and DS STG samples. The density of CR+ cells may be reduced in DS samples (control = $1.74 \times 10^6 \pm 0.14 \times 10^6$, DS = $1.19 \times 10^6 \pm 0.23 \times 10^6$, p = 0.11, N = 4), although a larger sample size is needed to reach statistical significance. To assess whether neuron counts correlate with post-mortem interval (PMI), independent of genotype, we performed a Pearson correlation analysis. The results show that there is no relationship between PMI and PV (0.05) but that there is a moderate relationship between PMI and NeuN (-0.41) and CR (-0.59). Despite these technical considerations, the results identify differences in the presence of interneuron subtypes, CR+ but not PV+, in adult DS cortex.

Ts21 iPSCs generate fewer CR+ neurons and fewer COUP-TFII+ progenitors

Our *in vivo* results corroborate historical data and suggest that the generation of cortical interneurons is altered by Ts21. Interneuron progenitors are specified and proliferate in the three neurogenic areas of the ventral telencephalon: the lateral, medial, and caudal ganglionic eminences

(LGEs, MGEs, and CGEs, respectively) (Anderson et al., 2002; Flames and Marin, 2005; Kessaris et al., 2014; Parnavelas et al., 2000; Xu et al., 2004). Individual spatially defined progenitor subpopulations with distinct transcriptional profiles each ultimately give rise to specific interneuron subtypes, thus initiating the diversity of interneurons in the cortex. MGE progenitors express the transcription factor *NKX2.1* and are the primary source of interneurons in mouse, giving rise to 70% of the total cortical interneurons including PV-, calbindin-, and somatostatin-expressing subtypes (Du et al., 2008; Xu et al., 2008, 2010). CGE progenitors express the transcription factor *COUP-TFII/NR2F2* that is also expressed by progenitors in the caudal MGE and along the MGE/LGE boundary (Kanatani et al., 2008). The CGE gives rise to vasoactive-intestinal-polypeptide-, CR-, reelin-, and neuropeptide-Y-expressing interneurons in mouse (Xu et al., 2004). Recent work indicates that these transcription factor codes are largely conserved between mouse and human, but human interneuron progenitors are more complex (Shi et al., 2021).

Here, we explore the development of human interneuron progenitors using iPSC modeling. Strategies to generate ventral neural progenitor cells (NPCs) and cortical interneurons from human pluripotent stem cells (hPSCs) (Kim et al., 2014; Liu et al., 2013; Maroof et al., 2013; Nicholas et al., 2013) rely on exogenous addition of sonic hedgehog (SHH) to specify progenitors to a ventral fate and yield a highly enriched population of GABA interneurons that mature to specific interneuron subtypes. One pair of isogenic Ts21 and control iPSCs (WC-24) were differentiated to cortical interneuron progenitors with exogenous SHH/purmorphamine from days 10–17 (Figure 2A; supplemental experimental procedures) (Liu et al., 2013). We previously reported the reduced generation of CR+ neurons from Ts21 progenitors using this paradigm (Huo et al., 2018). We repeated the experiment by maintaining our isogenic control and Ts21 interneuron progenitors for 74 or 91 days and then differentiating them to neurons to assess the generation of CR+ neurons. Quantification of CR+ neurons reveals reduced generation of CR+ neurons from Ts21 progenitors (Figure 2B), corroborating our previous results in distinct cell lines and confirming that we can model the decreased population of CR+ neurons in DS that we observe *in vivo* (Figure 1). Interneuron progenitors are specified temporally in addition to the spatial patterning that we are modeling in our culture system, and expression of subtype-specific markers *in vitro* appears after long-term culture, so we acknowledge that when counting at a particular time point, the number does not necessarily equal the progenitor population.

We focused on the specification of interneuron progenitors to gain insight into early developmental events that go awry in DS. NKX2.1+ and COUP-TFII+ populations are not mutually exclusive. While NKX2.1 is expressed in MGE, COUP-TFII is expressed in two spatial subpopulations of cortical interneuron progenitors: caudal MGE and CGE (Anderson, 2002; Anderson et al., 2002; Campbell, 2003; Parnavelas et al., 2000; Wilson and Rubenstein, 2000). These two COUP-TFII+ populations can be distinguished by NKX2.1 expression (Alfano et al., 2014; Kanatani et al., 2008; Lodato et al., 2011; Reinchisi et al., 2012); MGE progenitors express only NKX2.1, and CGE progenitors express only COUP-TFII, while caudal MGE progenitors express both. We differentiated four Ts21 iPSC and control iPSC lines (supplemental experimental procedures) using our paradigm (Figure 2A). To test whether Ts21 affects specification of interneuron progenitors, we quantified the subpopulations of progenitors. Immunofluorescence of progenitors at day 17 indicates that both control and Ts21 progenitors respond to SHH by expressing NKX2.1, as expected, as well as expressing COUP-TFII (Figure 2C). The percentage of MGE progenitors, as defined by NKX2.1+ COUP-TFII- expression, is not consistently different in Ts21 progenitors compared with isogenic or non-isogenic controls (control = 13.65 ± 11.40, Ts21 = 25.43 ± 6.49, $p = 0.1264$, $N = 4$) (Figure 2D). The proportion of NKX2.1+ COUP-TFII+ cells that represent caudal MGE-like cells is not statistically different between Ts21 iPSCs and controls (control = 20.28 ± 4.64, Ts21 = 9.632 ± 3.70, $p = 0.1232$, $N = 4$) (Figure 2D). The low proportion of NKX2.1+ MGE progenitors overall is likely related to the relatively late addition of SHH (at day 10) in our protocol. Quantification of COUP-TFII+ NKX2.1- cells that represent CGE-like progenitors revealed that fewer of these cells differentiate from Ts21 iPSCs compared with controls (control = 13.09 ± 0.72, Ts21 = 4.71 ± 1.12, $p = 0.0007$, $N = 4$) (Figure 2D). The results indicate that Ts21 progenitors generate fewer COUP-TFII+ cells.

Differences in expression of NKX2.1 and COUP-TFII expressing progenitors recapitulate *in vivo* development as there is decreased expression of *COUP-TFII/NR2F2*, but not *NKX2.1*, in human fetal DS brain (Olmos-Serrano et al., 2016) (Figure 2E). As COUP-TFII+ progenitors are an important source of CR interneurons in mice (Xu et al., 2004), the decreased generation of COUP-TFII+ progenitors from Ts21 iPSCs and the reduced expression of *COUP-TFII/NR2F* in DS fetal brain provide a potential mechanism for the decreased population of CR+ interneurons in DS.

Fewer Ts21 COUP-TFII+ progenitors are proliferating

Progenitors proliferate in response to extrinsic cues to expand the progenitor pool. We quantified proliferation of NPCs derived from three pairs of Ts21 and control iPSC lines by pulsing cells with 5-ethyl-2′-deoxyuridine (EdU) for 8 h to label dividing cells. We asked if the proportions of proliferating NKX2.1+ and COUP-TFII + cells

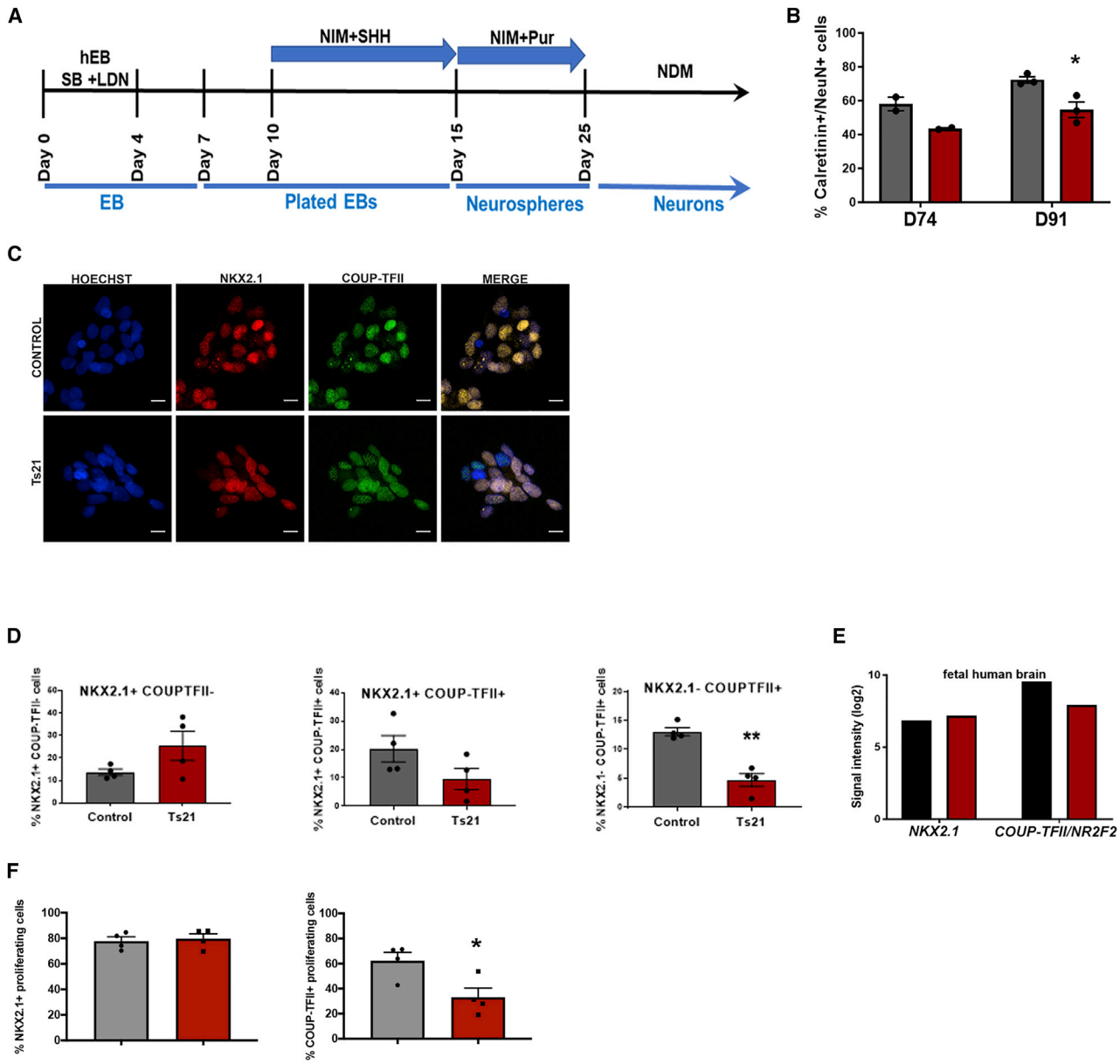

Figure 2. Ts21 iPSCs generate fewer CR+ interneurons and fewer COUP-TFII+ progenitors

(A) Interneuron progenitor differentiation protocol.

(B) Proportion of calretinin (CR) neurons/(NeuN+) differentiated from control and Ts21 progenitors at days 74 and 91. *p = 0.023 using unpaired t test with two-stage step up (Benjamini, Krieger, and Yekutieli).Control is black and Ts21 is red.

(C) Immunofluorescence images of NKX2.1+ and COUP-TFII+ nuclei in control and Ts21 neural progenitor cells (NPCs).

(D) Proportion of NKX2.1+ COUP-TFII- cells (MGE), NKX2.1+ COUP-TFII+ cells (caudal MGE), and NKX2.1- COUP-TFII+ cells (CGE) in control and Ts21 NPCs. **p < 0.001 using unpaired t test, N = 4 cell lines.

(E) Expression of NKX2.1 and COUP-TFII in human fetal control and DS brain (14–17 weeks gestation, dorsolateral forebrain) (Olmos-Serrano et al., 2016). Control is black and Ts21 is red.

(F) NKX2.1+/EdU+ and COUP-TFII+/EdU+ proliferating cells in the Ts21 cells compared with controls. *p < 0.05 using unpaired t test, N = 4.

differed between Ts21 and controls. Co-labeling of EdU+ cells with NKX2.1 or COUPTF-II shows no difference in the proportion of dividing NKX2.1+ cells in Ts21 (Figure 2F), indicating that the NKX2.1+ population is preserved in Ts21. In contrast, fewer dividing COUP-TFII+ cells are found in the Ts21 population than in controls

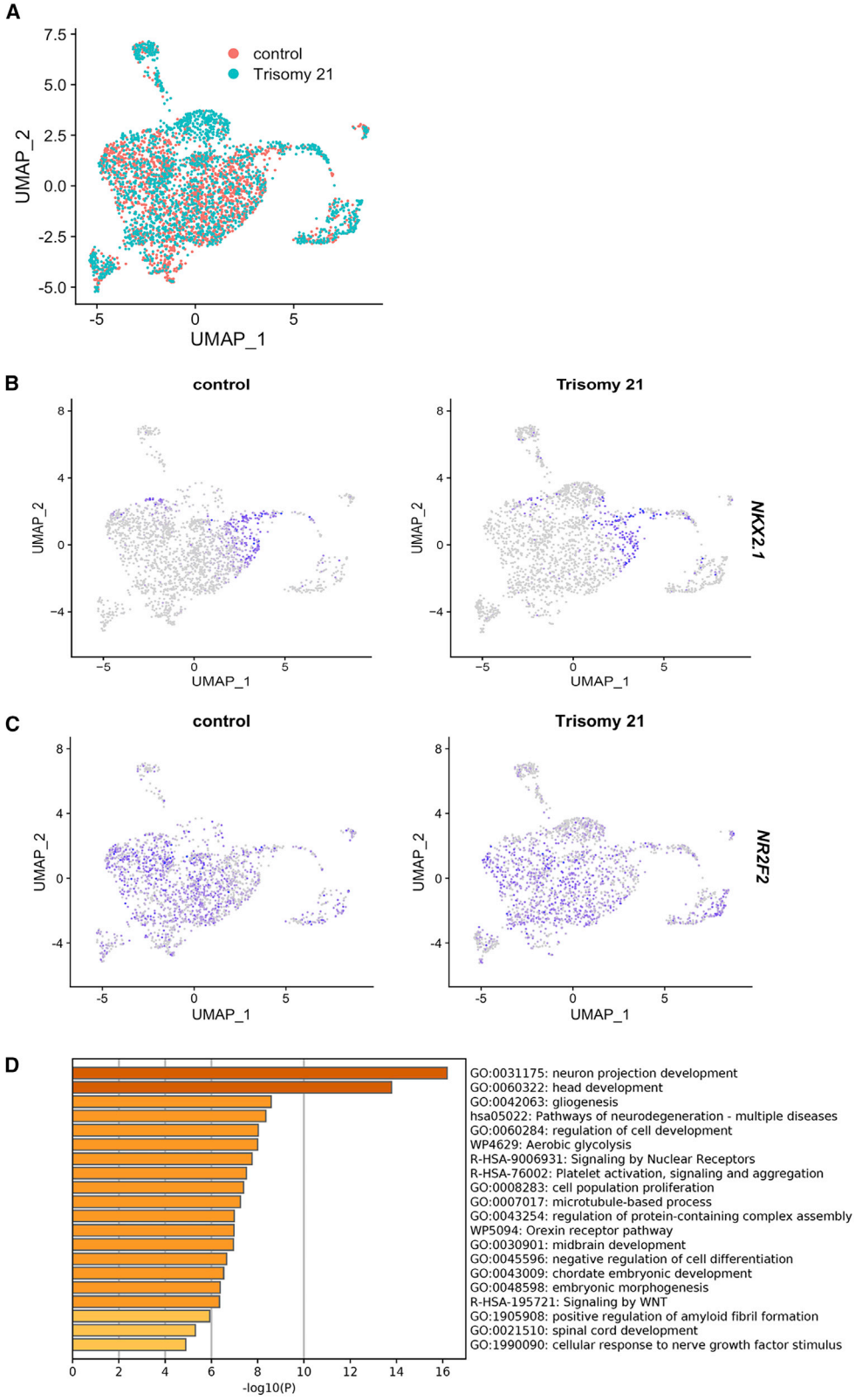

(legend on next page)

(Figure 2F). These data suggest that Ts21 COUP-TFII+ cells are either proliferating more slowly or exiting the cell cycle prematurely.

Single-cell transcriptomic analysis confirms cellular and molecular differences in Ts21 progenitors

To identify putative progenitor subpopulations that differ in Ts21 and to define gene pathways that are dysregulated by Ts21, we carried out single-cell RNA sequencing (scRNA-seq) analysis using ventralized progenitors at day 17 from one pair of isogenic Ts21 and control lines (WC-24). Isogenic pairs of iPSCs are extremely valuable for molecular profiling where variation between individuals and cell lines can be amplified and mask subtle differences.

As we are investigating an actively proliferating population of cells and because there are differences in the proliferation of Ts21 progenitors, cell-cycle genes are likely to be overrepresented in the analysis and therefore lead to clustering of cells based upon cell cycle rather than cellular fate. We used Seurat (v.4.0.4) to regress out cell-cycle genes so that the underlying gene markers could be used to segregate Ts21 and control cell populations (Butler et al., 2018; Mayer et al., 2018). The resulting unifold manifold approximation and projection (UMAP) plot shows that the euploid and Ts21 progenitors overlaid on each other, revealing similar populations in Ts21 and controls (Figure 3A). Feature plots of the data indicate that *NKX2-1* expression is restricted to a subset of clusters (Figure 3B). In contrast, *COUP-TFII/NR2F2* expression is widespread (Figure 3C), in agreement with widespread expression of *COUP-TFII/NR2F2* in fetal human ganglionic eminences (CGEs and LGEs) *in vivo* (Shi et al., 2021). The expression of these genes is thus different from protein expression (Figure 2).

Differentially expressed genes (DEGs) between Ts21 and control progenitor populations were identified using FindMarkers() function in Seurat with parameters logfc.threshold >0.25 and an adjusted p (padj) value of <0.05, and 206 DEGs were identified (Table S1). Pathway analysis of DEGs between Ts21 and control using Metascape (Zhou et al., 2019) indicates that genes involved in several neurodevelopmental processes are disrupted by Ts21 (Figures 3D; Tables S2 and S3). Association of DS and familial Alzheimer's disease with our data was validated using the DisGeNet database (Figure S1). Pathways, including both neurodevelopmental and neurodegenerative pathways, are driven by the increased expression of the chromosome-21-encoded gene *APP* in the Ts21 progenitors. Neurodevelopmental pathways emerge due to the altered expression of key transcription factors, including *FOXG1*, *DLX2*, *LHX2*, and *HES1*. WNT signaling emerges as an affected pathway driven by altered expression of non-chromosome 21 genes (*CALM2*, *SOX3*, *GNG2* and *GNG3*, *RSPO3* and *RSPO1*, *RAC1*, *PFN1* and *TCFL2*). *RSPO1* and *RSPO3*, context-dependent regulators of WNT signaling, are increased in Ts21 progenitors (Jin and Yoon, 2012; Rong et al., 2014), while *TCFL2*, a downstream effector gene (Chodelkova et al., 2018), is decreased. These single-cell data identify WNT as a dysregulated pathway in Ts21 interneuron progenitors.

Single-cell clustering reveals a GLI3-expressing subpopulation enriched in Ts21 progenitors

To identify putative progenitor subpopulations that differ in Ts21, we used Seurat to cluster the cells to reveal 15 subpopulations (Figure 4A). The identity of these cell populations was defined by identifying DEGs in each cluster with combined p values less than 0.05 (Table S4; Figure S2). We cross-referenced these gene signatures to known gene markers of NPC populations to classify each population. The clustered cell types expressed genes indicative of cells at different stages of differentiation and different progenitor populations, revealing the heterogeneity of our iPSC-derived progenitors. We also compared cluster marker expression in our cells with clusters of human fetal ganglionic eminences (Shi et al., 2021) and found widespread expression overlap, validating that our progenitors have similar gene expression as fetal tissue (Figure S3). Similar proportions of control and Ts21 cells were represented in each subpopulation (Figure 4B). However, quantification of the number of cells in each cluster revealed that one cluster, cluster 3, was enriched in Ts21 (Figure 4C). This cluster is identified by expression of *FOXG1* and the long non-coding RNA LINC00551 (Figure 4D; Table S4). Interestingly, *GLI3* is a unique marker gene for cluster 3 (Figure 4E; Table S4). *GLI3*, as well as other marker genes in this cluster (*FOXG1*, *LHX2*, *MEIS2*), is highly expressed in intermediate progenitor cells in fetal brain (Li et al., 2018) and thus confirms the identity of cluster 3 as a population of intermediate progenitors.

DEGs between Ts21 and control cells in cluster 3 were identified using the FindMarkers() function in Seurat with parameters logfc.threshold >0.25 and a padj value of <0.05, and 72 DEGs were identified (Table S5). Pathway analysis of these DEGs using Metascape (Zhou et al., 2019) indicates that genes involved in several cellular processes are disrupted by Ts21 (Figures 4F; Table S6). Enriched expression of

Figure 3. Single-cell RNA-seq reveals gene-expression differences in Ts21 progenitors

(A) Dimensional reduction by experimental group (control and Ts21).

(B) Feature plot of expression of NKX2.1 in control and trisomy cells.

(C) Feature plot of expression of COUP-TFII/NR2F2 in control and trisomy cells.

(D) Pathway analysis of differentially expressed genes in Ts21 compared with control.

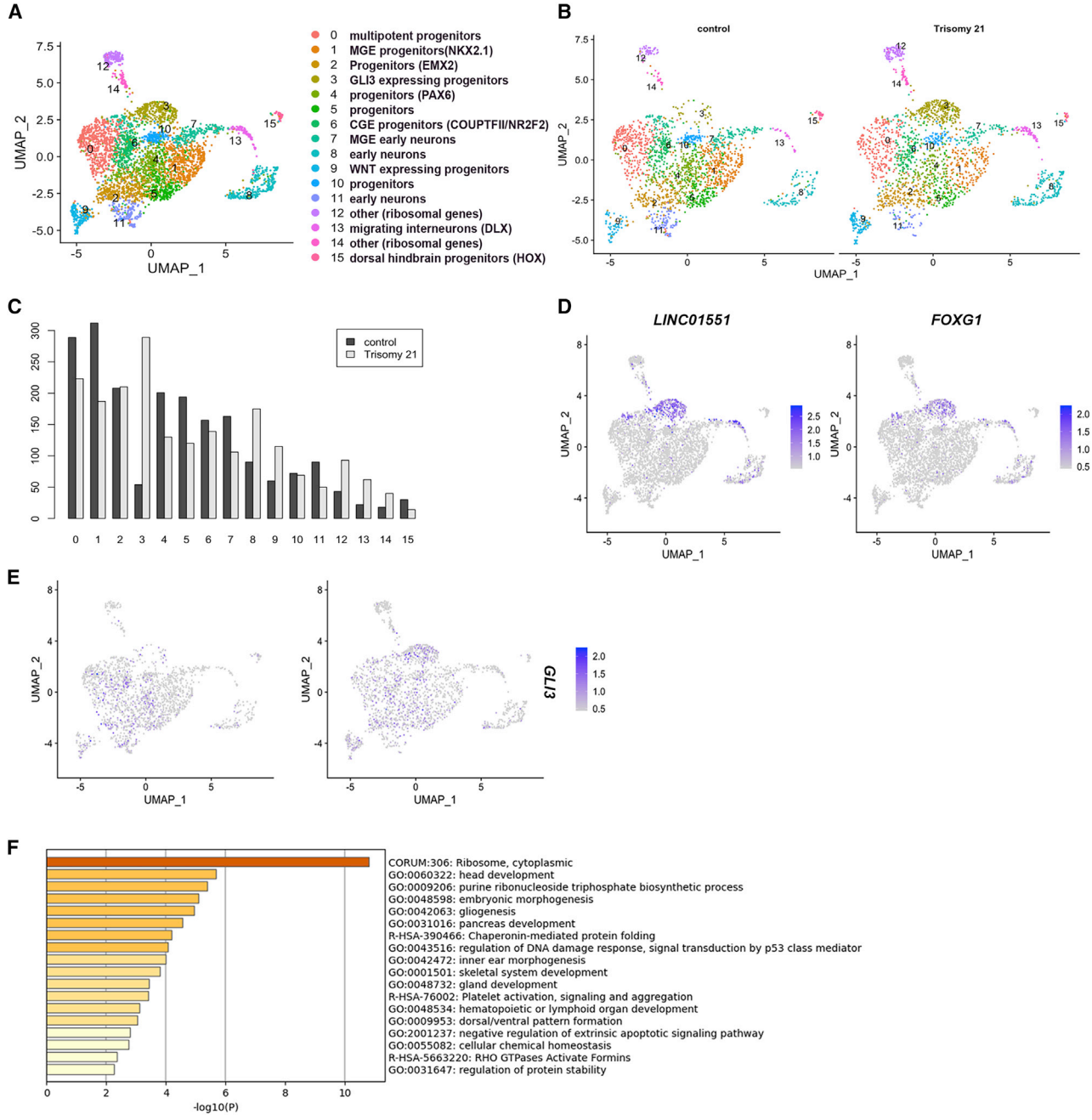

Figure 4. Single-cell RNA-seq reveals differences in Ts21 progenitor clustering

(A) Clustering analysis revealed 15 subpopulations of cells based on expression of known gene markers.

(B) Clustering of control (2,134 cells) and Ts21 (2,158 cells).

(C) Proportion of control and Ts21 cells in each cluster reveals enrichment of cluster 3 in Ts21 cells.

(D) Feature plot of LINC0551 and FOXG1, markers that identify cluster 3 (Table S4).

(E) Feature plot showing expression of GLI3.

(F) Pathway analysis of differentially expressed genes in cluster 3 in Ts21 compared with control.

ribosomal genes (*RPL37A*, *RPL4*) in Ts21 cells drives the identification of the top pathway of ribosome/translation. These genes are also enriched in intermediate progenitors (Li et al., 2018). DEGs in cluster 3 include downregulation of WNT pathway genes in Ts21 (*TCF7L2*, *SOX4*, *GNG3* and *GNG5*, and *GPC3*). Together, these data raise the hypothesis that

cluster 3 arises from Ts21 progenitors due to decreased WNT signaling.

Ts21 progenitors exhibit reduced WNT and upregulated GLI expression that can be rescued by WNT activation

Cellular analysis of multiple pairs of Ts21 and control lines indicate that the specification and proliferation of a specific progenitor pool (COUP-TFII+) is altered in Ts21 (Figure 2), and scRNA-seq data identifies dysregulated WNT signaling in Ts21 progenitors (Figure 3). WNT and its antagonist SHH precisely mediate the specification and proliferation of cortical interneuron progenitors (Gulacsi and Anderson, 2006; Li et al., 2009; Xu et al., 2005). Thus, the reduced proportion of COUP-TFII+ cells in Ts21 could be due to a failure to respond to WNT. We therefore tested whether the expression of SHH and WNT pathway genes was reduced in Ts21 progenitors using quantitative PCR for specific pathway genes in two sets of isogenic progenitors. We confirmed that while expression of SHH pathway genes was not consistently different in Ts21 progenitors (Figure 5A), expression of WNT pathway genes was reduced in Ts21 progenitors (Figure 5B). A comparison with the expression of these genes in human fetal brain indicated that the WNT target gene *AXIN2*, but not other components of the SHH or WNT pathways, was also reduced in DS fetal brain (Olmos-Serrano et al., 2016) (Figure 5C). These results corroborate that Ts21 progenitors have defects in WNT-signaling machinery.

We next assessed the expression of GLI genes and found that expression of *GLI3* was increased in Ts21 progenitors, in agreement with increased expression in human fetal DS brain (Figure 5D). Enrichment of a *GLI3*-expressing cluster of progenitors in Ts21 (Figures 4C and 4E) provides an explanation for the increased *GLI3* expression.

To test whether activation of WNT can rescue the decreased population of COUP-TFII+ cells in Ts21, we tested the response of Ts21 ventral progenitors to WNT. Activation of WNT via addition of a WNT agonist (CHIR) with SHH moderately increases both *COUP-TFII*/*NR2F2* expression and the proportion of COUP-TFII+ cells in Ts21 progenitors (Figure 5E). Importantly, WNT activation also decreases the overexpression of *GLI3* in Ts21 progenitors (Figure 5F), suggesting that the enriched cluster 3 arises from Ts21 progenitors due to decreased WNT signaling. These data support a proposed mechanism in which deficient WNT signaling in Ts21 progenitors leads to a change in specification (and possibly proliferation) of Ts21 progenitors.

DISCUSSION

Fewer CR neurons in DS

Expansion of upper layers of the cortex in primates includes more excitatory neurons in layers II and III, and there may also need to be a compensatory inhibitory neuron expansion. CR+ neurons are predominantly found in upper layers of the cortex, and, in primates, a greater proportion of interneurons are CR+ neurons (Dzaja et al., 2014; Hansen et al., 2013; Hladnik et al., 2014; Ma et al., 2013). Our results align with this idea as we find a larger proportion of CR+ neurons compared with PV+ neurons in the human STG (Figure 1).

By carefully assessing interneurons in post-mortem adult brain, we show that at least one interneuron subtype population, CR+, is reduced in DS. Reduced density of neurons could be due to degeneration in adulthood. However, we selected samples from 15- to 35-year-old individuals with DS, before neuronal degeneration is thought to take place. In fact, reduced neuron density has been reported in fetal DS brain (Golden and Hyman, 1994; Guidi et al., 2018; Larsen et al., 2008; Schmidt-Sidor et al., 1990; Stagni et al., 2018). In particular, Guidi et al. reported fewer CR+ cells in human fetal DS cortex in the fusiform and inferior temporal gyri (Guidi et al., 2018), corroborating our adult data and supporting the idea that this population is affected during development.

Our data are consistent with the predominant candidate mechanism underlying intellectual disability in DS that has emerged from mouse models of an imbalance in excitation-inhibition in the cortex, specifically over-inhibition, which has led to the targeting of over-inhibition in the cortex by various drugs (Deidda et al., 2015; Gardiner, 2010; Martinez-Cue et al., 2014; Potier et al., 2014; Zorrilla de San Martin et al., 2018). While the decrease in interneurons that we observe may seem contrary to this hypothesis, CR+ interneurons function in disinhibitory circuits (Guet-McCreight et al., 2020; Pi et al., 2013) that specialize in inhibiting GABA interneurons. Fewer CR+ neurons in DS could provide less inhibition and thus increased activity of inhibitory GABA interneurons to elicit over-inhibition.

Specification of interneuron progenitors is altered by Ts21

Using disorder-specific iPSCs, we investigated if and how early events in interneuron development are altered in DS. At the cellular level, we corroborate that we can model the reduced generation of CR+ interneurons *in vitro*. Results indicate that NKX2.1+ MGE progenitors are not altered but that fewer COUP-TFII+ progenitors are generated in Ts21. Our data appear to differ from a report that concluded that more NKX2.1+ progenitors and more interneurons are generated from Ts21 iPSCs (Xu et al., 2019). Besides difference in the use of 3D versus 2D cultures, we take an unbiased approach to assess interneuron progenitors from Ts21 iPSCs, while Xu et al. analyzed OLIG2+ cells. In addition, we are looking at an early time point when

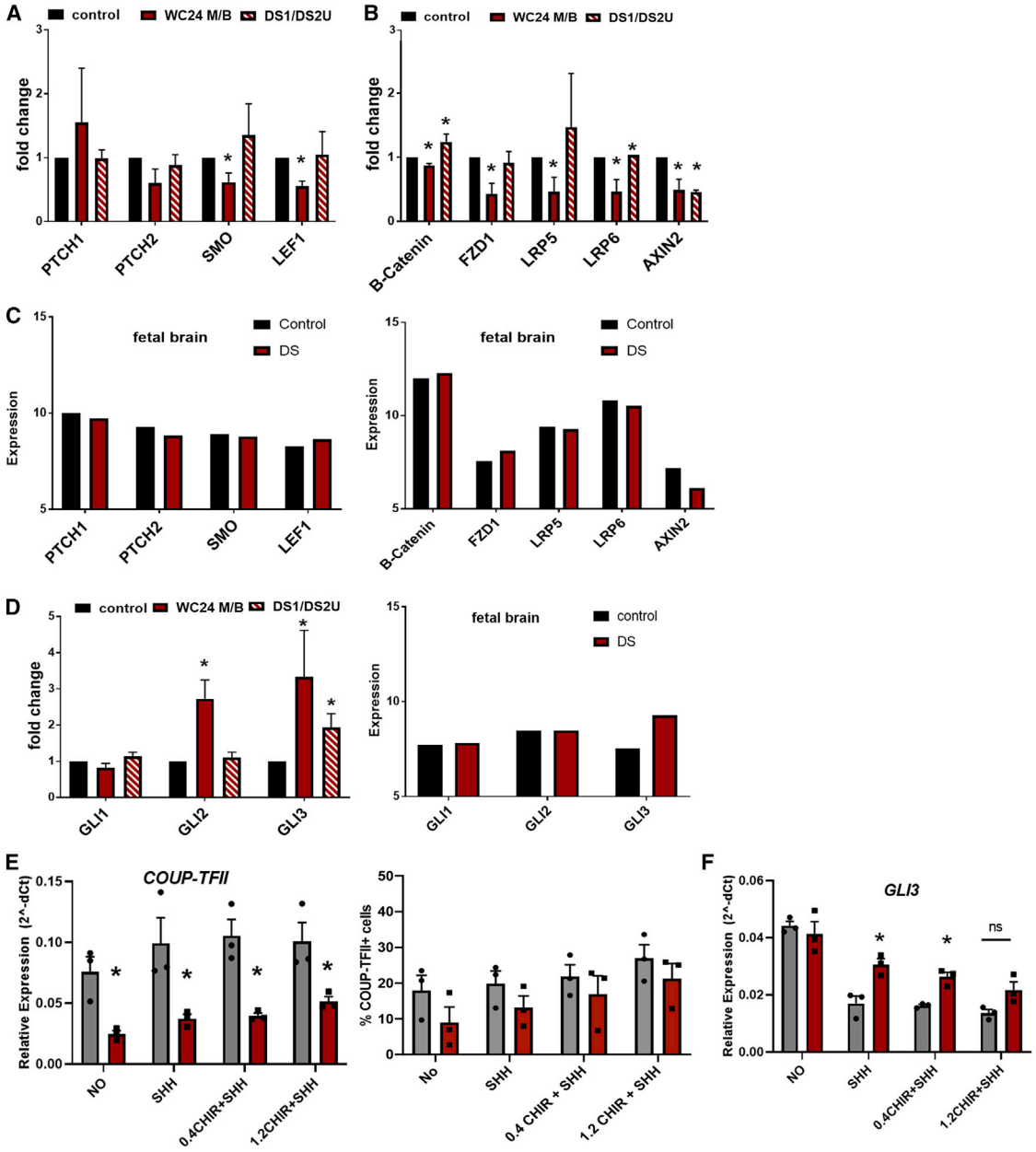

Figure 5. Ts21 ventral progenitors have decreased WNT and increased GLI3 expression

(A and B) Quantitative PCR of SHH pathway genes (A) WNT signaling genes (B) in two iPSC lines of Ts21 and isogenic control lines.

(C) Expression of SHH and WNT pathway genes in human fetal control and DS brain (14–17 weeks gestation, dorsolateral forebrain, Olmos-Serrano et al., 2016).

(D) Quantitative PCR of GLI genes in progenitor cells and in human fetal control and DS brain (Olmos-Serrano et al., 2016). Statistical significance was determined by one-sample t test on ddCt values. *$p < 0.05$, N = 3 for each gene/line.

(E) The effects of activation of WNT via addition of a WNT agonist (CHIR, 0.4 and 1.2 μm) with SHH on COUP-TFII/NR2F2 gene expression, proportion of COUP-TFII+ cells, and GLI3 expression. Statistical significance was determined by one-sample t test on ddCt values. *$p < 0.05$, N = 3 replicates in one pair of isogenic control and Ts21 cells.

progenitors have established their positional identity, while Xu et al. analyzed a later time point. Thus, we may be assessing different progenitor populations.

In mouse, CR+ interneurons derive from COUP-TFII+ progenitors, and so these results link the altered development of the COUP-TFII+ subpopulation *in vitro* with fewer

CR+ interneurons that we observe both *in vitro* and *in vivo* (Huo et al., 2018). Yet, the origin of CR+ neurons has not been established in human, and it is possible that some of the NKX2.1+ MGE cells also give rise to CR+ cells. CR+ neurons primarily populate upper layers of the cortex and thus are likely derived from late-born COUP-TFII+ progenitors. It is also possible that specification of CR+ neurons is from MGE initially and CGE later and that decreased pools of CGE progenitors affect late-born neurons.

Our data suggest potential cellular mechanisms underlying the observed decrease in COUP-TFII+ progenitors in Ts21. Ts21 progenitors could have altered specification, supported by the enrichment of a specific subpopulation of progenitors revealed by our single-cell clustering. Proliferation changes during development also contribute to the decreased neuronal numbers and reduced cortical volume in DS brain (Contestabile et al., 2007; Guidi et al., 2011). The decreased number of proliferating COUP-TFII+ cells in Ts21 supports the pre-mature exit of COUP-TFII+ cells from the cell cycle. These mechanisms are not mutually exclusive but can be addressed through lineage tracing of COUP-TFII+ progenitors.

Single-cell transcriptomics reveal that ventralized progenitors differentiated from iPSCs are heterogeneous, complicating our ability to match cellular phenotypes with molecular signatures. In particular, *COUP-TFII/NR2F2* expression in human is more complex than in mouse. Recent data from Shi et al. indicates that *PAX6*, *MEIS2*, and *COUP-TFII/NR2F2* expression is widespread in CGE and LGE, contrary to the prevailing ideas that PAX6 expression is limited to dorsal NPCs, that MEIS2 is a marker of LGE, and that *COUP-TFII/NR2F2* is a marker of CGE (Shi et al., 2021). Further, Shi et al. uncovered a cluster of *COUP-TFII/NR2F2* cells that are unique to human. A deeper understanding of the effects of Ts21 on interneuron progenitor specification requires single-cell analysis of developing DS tissue.

Cells in the Ts21-enriched cluster express markers that identify them as intermediate progenitor cells (Li et al., 2018). The presence of this cluster could indicate that Ts21 interneuron progenitors differentiate more slowly than controls and are thus retained in this intermediate stage. *GLI3* is mis-expressed temporally during fetal cortical development; *GLI3* expression is initially higher than controls and then lower than controls (Olmos-Serrano et al., 2016), consistent with altered emergence of this cluster of cells. Alternatively, this developmental cluster could represent an alternative differentiation pathway taken by Ts21 progenitors. These different scenarios can be tested through single-cell analysis across developmental times, either *in vivo* or *in vitro*.

Ts21 progenitors have reduced WNT signaling

Ts21 progenitors could have altered specification due to a reduced ability to respond to WNT, as supported by the enrichment of cluster 3 and altered WNT pathway genes in Ts21. WNT signaling has been implicated in other cellular mechanisms associated with aging and neuropathology in DS (Adorno et al., 2018; Cairney et al., 2009; Granno et al., 2019). Since WNT is used in a tightly regulated and spatially specific manner during forebrain development to regulate regional identity, it is likely that decreased WNT signaling in Ts21 would have an impact on neurodevelopment. Our molecular data suggest that altered specification of Ts21 progenitors is at least partly due to decreased WNT signaling, which is corroborated by the restoration of the COUP-TFII+ progenitor subpopulation and *GLI3* expression through WNT activation. These data raise the hypothesis that Ts21 *GLI3*-expressing intermediate progenitors in cluster 3 emerge due to reduced WNT responsiveness. It will be important to test whether WNT activation can specifically eliminate cluster 3 and/or whether other progenitor subpopulations are affected by WNT activation through additional single-cell analyses.

EXPERIMENTAL PROCEDURES

Quantification of neurons in post-mortem brain

Tissue

Post-mortem brain tissue was obtained from the NICHD Brain and Tissue Bank for Developmental Disorders (Neurobiobank) with approval from the University of Wisconsin-Madison Human Subjects IRB. STG or Brodmann area 22 was obtained from 4 individuals with DS and was age and gender matched with control subjects (supplemental experimental procedures).

Immunocytochemistry

Tissues were cryosectioned at 50 μm and processed for immunocytochemistry. Antigen-antibodies were visualized with avidin-biotin, horseradish peroxidase (HRP), and 3,3′-diaminobenzidine (DAB) using standard immunohistochemical techniques on floating sections (supplemental experimental procedures).

Quantification of positive cells

Total numbers of NeuN+, PV+, CR+, and SST+ neurons were estimated using the Optical Fractionator (OF) workflow in Stereo Investigator software (MBF Bioscience). The total cell population estimate (from the OF Workflow) was divided by the total tissue volume (from the Cavalieri Estimator) to calculate cell density.

Human iPSCs

iPSCs

We used two Ts21 iPSC isogenic pairs and additional iPSCs from individuals with DS and unaffected controls (supplemental experimental procedures). Primary dermal fibroblasts were isolated from tissue acquired with approval from the University of Wisconsin-Madison Human Subjects IRB (protocol #2016–0979). Fibroblasts were reprogrammed by electroporation delivery of episomal vectors pCXLE-hOCT3/4-shp53-F (Addgene, 27077), pCXLE-hSK (Addgene, 27078), and pCXLE-hUL (Addgene, 27080). The iPSC colonies were manually picked between days 14 and 28

post-transfection. Following expansion, cells were transferred onto matrigel (R&D) and cultured with mTeSR1 (Stemcell Technologies) for banking.

Cell culture

iPSCs were maintained on murine embryonic fibroblasts (MEFs) in human embryonic stem cell (hESC) media (DMEM/F-12/KOSR/L-Glut/MEM-NEAA/FGF-2) and passaged with collagenase. Differentiation to interneuron progenitors was carried out as described (Liu et al., 2013) using SHH as a morphogen and maintaining neurospheres in NIM with B27 and purmorphamine.

Cellular analysis

Cell proliferation

Cell proliferation was assayed using Click-iT EdU Alexa Fluor 488 Imaging Kit. EdU was added to cells for 8 h. Cells were fixed with 4% paraformaldehyde in PBS for 15 min and processed for immunofluorescence.

Immunofluorescence

NPCs were plated onto laminin coated 96-well cell culture plates or coverslips at 50–60,000 cells/well/coverslip. The day after plating, cells were fixed with 4% paraformaldehyde and processed for immunofluorescence.

High-content imaging analysis

Imaging and analysis were done using the high-content imager Operetta (Perkin Elmer) at 20 × magnification.

Molecular analysis

qPCR

qPCR was performed in triplicate on 2–3 batches of differentiation (N = 3) (supplemental experimental procedures). Data are presented as fold change calculated from ddCt values. Error bars indicate fold change of ddCt values ± 1 SD. Statistical significance was determined by one-sample t test on ddCt values.

scRNA-seq

NPCs were analyzed using the 10X Genomics Chromium Single-Cell Gene Expression Assay at the University of Wisconsin Biotechnology Center. Sequence data was analyzed on servers at the UW-Madison Bioinformatics Resources Center remotely via Bash UNIX shell commands. Raw read quality was confirmed with FastQC Processing. The 10X Genomics pipeline linux commands were used for processing the data for analysis. Briefly, Cell Ranger mkfastq was used to demultiplex the raw read files into FastQ files. The FastQ files were then passed on to Cell Ranger count for alignment, filtering, barcode counting, and unique molecular identifier (UMI) counting.

The processed count matrix contains 33,694 genes and 2,134 cells in the control group and 2,158 cells in the Ts21 group, respectively. We used Seurat 4.0.4 for downstream analysis. First, we filtered cells that detected unique genes less than 20 or over 10^5 and then filtered cells that had more than 5% mitochondrial counts. After filtering, the dataset retains 4,025 cells (control: 2,003; Ts21: 2,022). Second, we normalized the data and found the top 2,000 highly variable genes using Seurat. We implemented integrated analysis for the two samples. Then, we mitigated the effects of cell-cycle heterogeneity in the dataset by calculating cell-cycle phase scores based on canonical markers and regressing these out of the data. Next, we performed principal-component analysis (PCA) for dimension reduction on the integrated dataset for later clustering and visualization. Code is available in supplemental experimental procedures.

Statistics

Experiments include three biological replicates (batches of differentiation, N = 3 or individual cell lines N = 3 or 4) and 3 technical replicates (n = 3) for each cell line. Ts21 and control pairs were differentiated together. Data were analyzed using GraphPad Prism v.8. All pooled data are presented as mean + standard error of the mean (SEM). Differences were considered statistically significant at $p < 0.05$.

Data and code availability

scRNA-seq data GEO: GSE201523.

SUPPLEMENTAL INFORMATION

Supplemental information can be found online at https://doi.org/10.1016/j.stemcr.2022.05.001.

AUTHOR CONTRIBUTIONS

Conceptualization, A.B. and S.-C.Z.; methodology, Y.G.-R., J.S., B.S., M.M., and D.W.; software and data curation, Y.G.-R., J.S., and D.W.; investigation, Y.G.-R., J.S., B.S., K.X., L.H., M.M., K.A.R., S.D., S.M., A.K., R.A.D., Jr., B.L., L.A., and R.R.; writing – original draft, Y.G.-R. and A.B.; writing – review & editing, A.B., Y.T., A.S., and S.-C.Z.; funding acquisition, project administration, resources, and supervision, A.B., S.-C.Z., and D.W.

CONFLICTS OF INTEREST

S.-C.Z. is a co-founder of BrainXell, Inc. The other authors declare no competing interests.

ACKNOWLEDGMENTS

We thank members of the A.B. and S.-C.Z. labs for helpful comments and technical assistance. We thank Karla Knobel, Emily Fares, Anna Baker, MBF technical support, Manuel Casanova, and Kenneth Fish for guidance on stereology. This study utilized the University of Wisconsin-Madison Biotechnology Center's Gene Expression Center Core Facility (Research Resource Identifier [RRID]: SCR_017757) for single-cell RNA library preparation and the DNA Sequencing Facility (RRID: SCR_017759) for sequencing, and we thank S. Splinter-BonDurant, D. Pavelec, and M.E. Berres for technical assistance. This work was supported by NIH grants R03HD083538 and R21NS105339 to A.B. and 1R01HD106197 to A.B. and S.-C.Z. and by funding from UW-Madison and the Wisconsin Alumni Research Foundation to A.B. and, in part, by a core grant to the Waisman Center from the National Institute of Child Health and Human Development (U54 HD090256).

Received: July 24, 2020
Revised: May 1, 2022
Accepted: May 2, 2022
Published: May 26, 2022

REFERENCES

Adorno, M., di Robilant, B.N., Sikandar, S.S., Acosta, V.H., Antony, J., Heller, C.H., and Clarke, M.F. (2018). Usp16 modulates Wnt signaling in primary tissues through Cdkn2a regulation. Sci. Rep. *8*, 17506.

Alfano, C., Magrinelli, E., Harb, K., and Studer, M. (2014). The nuclear receptors COUP-TF: a long-lasting experience in forebrain assembly. Cell Mol. Life Sci. *71*, 43–62.

Anderson, S.A. (2002). Determination of cell fate within the telencephalon. Chem. senses *27*, 573–575.

Anderson, S.A., Kaznowski, C.E., Horn, C., Rubenstein, J.L.R., and McConnell, S.K. (2002). Distinct origins of neocortical projection neurons and interneurons in vivo. Cereb. Cortex. *12*, 702–709.

Arshad, A., Vose, L.R., Vinukonda, G., Hu, F., Yoshikawa, K., Csiszar, A., Brumberg, J.C., and Ballabh, P. (2016). Extended Production of cortical Interneurons into the third Trimester of human gestation. Cereb. Cortex *26*, 2242–2256.

Becker, L.E. (1991). Synaptic dysgenesis. Can. J. Neurol. Sci. *18*, 170–180.

Becker, L.E., Mito, T., Takashima, S., and Onodera, K. (1991). Growth and development of the brain in Down syndrome. Prog. Clin. Biol. Res. *373*, 133–152.

Benda, C.E. (1947). Mongolism and Cretinism (Grune and Stratton).

Bhattacharyya, A., McMillan, E., Chen, S.I., Wallace, K., and Svendsen, C.N. (2009). A critical period in cortical interneuron neurogenesis in Down syndrome revealed by human neural progenitor cells. Dev. Neurosci. *31*, 497–510.

Boyce, R.W., Dorph-Petersen, K.A., Lyck, L., and Gundersen, H.J.G. (2010). Design-based stereology: introduction to basic concepts and practical approaches for estimation of cell number. Toxicol. Pathol. *38*, 1011–1025.

Butler, A., Hoffman, P., Smibert, P., Papalexi, E., and Satija, R. (2018). Integrating single-cell transcriptomic data across different conditions, technologies, and species. Nat. Biotechnol. *36*, 411–420.

Cairney, C.J., Sanguinetti, G., Ranghini, E., Chantry, A.D., Nostro, M.C., Bhattacharyya, A., Svendsen, C.N., Keith, W.N., and Bellantuono, I. (2009). A systems biology approach to Down syndrome: identification of Notch/Wnt dysregulation in a model of stem cells aging. Biochim. Biophys. Acta *1792*, 353–363.

Campbell, K. (2003). Dorsal-ventral patterning in the mammalian telencephalon. Curr. Opin. Neurobiol. *13*, 50–56.

Chodelkova, O., Masek, J., Korinek, V., Kozmik, Z., and Machon, O. (2018). Tcf7L2 is essential for neurogenesis in the developing mouse neocortex. Neural Dev. *13*, 8.

Colon, E.J. (1972). The structure of the cerebral cortex in Down's Syndrome: a quantitative analysis. Neuropadiatrie *3*, 376.

Contestabile, A., Fila, T., Ceccarelli, C., Bonasoni, P., Bonapace, L., Santini, D., Bartesaghi, R., and Ciani, E. (2007). Cell cycle alteration and decreased cell proliferation in the hippocampal dentate gyrus and in the neocortical germinal matrix of fetuses with Down syndrome and in Ts65Dn mice. Hippocampus *17*, 665–678.

Davidoff, L.M. (1928). The brain in Mongolian idiocy: a report of ten cases. Arch. Neurol. Psychiatry *20*, 1229.

Deidda, G., Parrini, M., Naskar, S., Bozarth, I.F., Contestabile, A., and Cancedda, L. (2015). Reversing excitatory GABAAR signaling restores synaptic plasticity and memory in a mouse model of Down syndrome. Nat. Med. *21*, 318–326.

Du, T., Xu, Q., Ocbina, P.J., and Anderson, S.A. (2008). NKX2.1 specifies cortical interneuron fate by activating Lhx6. Development *135*, 1559–1567.

Dzaja, D., Hladnik, A., Bicanic, I., Bakovic, M., and Petanjek, Z. (2014). Neocortical calretinin neurons in primates: increase in proportion and microcircuitry structure. Front. Neuroanat. *8*, 103.

Emerson, J.F., Kesslak, J.P., Chen, P.C., and Lott, I.T. (1995). Magnetic resonance imaging of the aging brain in Down syndrome. Prog. Clin. Biol. Res. *393*, 123–138.

Flames, N., and Marin, O. (2005). Developmental mechanisms underlying the generation of cortical interneuron diversity. Neuron *46*, 377–381.

Gardiner, K.J. (2010). Molecular basis of pharmacotherapies for cognition in Down syndrome. Trends Pharmacol. Sci. *31*, 66–73.

Golden, J.A., and Hyman, B.T. (1994). Development of the superior temporal neocortex is anomalous in trisomy 21. J. Neuropathol. Exp. Neurol. *53*, 513–520.

Granno, S., Nixon-Abell, J., Berwick, D.C., Tosh, J., Heaton, G., Almudimeegh, S., Nagda, Z., Rain, J.C., Zanda, M., Plagnol, V., et al. (2019). Downregulated Wnt/β-catenin signalling in the Down syndrome hippocampus. Sci. Rep. *9*, 7322.

Guet-McCreight, A., Skinner, F.K., and Topolnik, L. (2020). Common Principles in functional Organization of VIP/calretinin cell-driven disinhibitory circuits across cortical areas. Front. Neural Circuits *14*, 32.

Guidi, S., Ciani, E., Bonasoni, P., Santini, D., and Bartesaghi, R. (2011). Widespread proliferation impairment and hypocellularity in the cerebellum of fetuses with down syndrome. Brain Pathol. *21*, 361–373.

Guidi, S., Giacomini, A., Stagni, F., Emili, M., Uguagliati, B., Bonasoni, M.P., and Bartesaghi, R. (2018). Abnormal Development Of The Inferior Temporal Region In Fetuses With Down Syndrome. Brain Pathol. *28*, 986–998.

Gulacsi, A., and Anderson, S.A. (2006). Shh maintains Nkx2.1 in the MGE by a Gli3-independent mechanism. Cereb. Cortex *16*, 89–95.

Hansen, D.V., Lui, J.H., Flandin, P., Yoshikawa, K., Rubenstein, J.L., Alvarez-Buylla, A., and Kriegstein, A.R. (2013). Non-epithelial stem cells and cortical interneuron production in the human ganglionic eminences. Nat. Neurosci. *16*, 1576–1587.

Hartley, S.L., Handen, B.L., Devenny, D.A., Hardison, R., Mihaila, I., Price, J.C., Cohen, A.D., Klunk, W.E., Mailick, M.R., Johnson, S.C., and Christian, B.T. (2014). Cognitive functioning in relation to brain amyloid-beta in healthy adults with Down syndrome. Brain. *137*, 2556–2563.

Hladnik, A., Dzaja, D., Darmopil, S., Jovanov-Milosevic, N., and Petanjek, Z. (2014). Spatio-temporal extension in site of origin for cortical calretinin neurons in primates. Front. Neuroanat. *8*, 50.

Huo, H.Q., Qu, Z.Y., Yuan, F., Ma, L., Yao, L., Xu, M., Hu, Y., Ji, J., Bhattacharyya, A., Zhang, S.C., and Liu, Y. (2018). Modeling

down Syndrome with Patient iPSCs reveals Cellular and migration Deficits of GABAergic neurons. Stem Cell Rep. *10*, 1251–1266.

Jin, Y.R., and Yoon, J.K. (2012). The R-spondin family of proteins: emerging regulators of WNT signaling. Int. J. Biochem. Cell Biol. *44*, 2278–2287.

Jones, E.G. (2009). The origins of cortical interneurons: mouse versus monkey and human. Cereb. Cortex *19*, 1953–1956.

Kanatani, S., Yozu, M., Tabata, H., and Nakajima, K. (2008). COUP-TFII is preferentially expressed in the caudal ganglionic eminence and is involved in the caudal migratory stream. J. Neurosci. *28*, 13582–13591.

Kessaris, N., Magno, L., Rubin, A.N., and Oliveira, M.G. (2014). Genetic programs controlling cortical interneuron fate. Curr. Opin. Neurobiol. *26*, 79–87.

Kesslak, J.P., Nagata, S.F., Lott, I., and Nalcioglu, O. (1994). Magnetic resonance imaging analysis of age-related changes in the brains of individuals with Down's syndrome. Neurology *44*, 1039–1045.

Kim, T.G., Yao, R., Monnell, T., Cho, J.H., Vasudevan, A., Koh, A., Peeyush, K.T., Moon, M., Datta, D., Bolshakov, V.Y., et al. (2014). Efficient specification of interneurons from human pluripotent stem cells by dorsoventral and rostrocaudal modulation. Stem. Cells. *32*, 1789–1804.

Larsen, K.B., Laursen, H., Graem, N., Samuelsen, G.B., Bogdanovic, N., and Pakkenberg, B. (2008). Reduced cell number in the neocortical part of the human fetal brain in Down syndrome. Ann. Anat. *190*, 421–427.

Li, M., Santpere, G., Imamura Kawasawa, Y., Evgrafov, O.V., Gulden, F.O., Pochareddy, S., Sunkin, S.M., Li, Z., Shin, Y., Zhu, Y., et al. (2018). Integrative functional genomic analysis of human brain development and neuropsychiatric risks. Science *362*, eaat7615.

Li, X.J., Zhang, X., Johnson, M.A., Wang, Z.B., Lavaute, T., and Zhang, S.C. (2009). Coordination of sonic hedgehog and Wnt signaling determines ventral and dorsal telencephalic neuron types from human embryonic stem cells. Development *136*, 4055–4063.

Liu, Y., Liu, H., Sauvey, C., Yao, L., Zarnowska, E.D., and Zhang, S.C. (2013). Directed differentiation of forebrain GABA interneurons from human pluripotent stem cells. Nat. Protoc. *8*, 1670–1679.

Lodato, S., Tomassy, G.S., De Leonibus, E., Uzcategui, Y.G., Andolfi, G., Armentano, M., Touzot, A., Gaztelu, J.M., Arlotta, P., Menendez de la Prida, L., and Studer, M. (2011). Loss of COUP-TFI alters the balance between caudal ganglionic eminence- and medial ganglionic eminence-derived cortical interneurons and results in resistance to epilepsy. J. Neurosci. *31*, 4650–4662.

Lott, I.T., and Dierssen, M. (2010). Cognitive deficits and associated neurological complications in individuals with Down's syndrome. Lancet Neurol. *9*, 623–633.

Ma, T., Wang, C., Wang, L., Zhou, X., Tian, M., Zhang, Q., Zhang, Y., Li, J., Liu, Z., Cai, Y., et al. (2013). Subcortical origins of human and monkey neocortical interneurons. Nat. Neurosci. *16*, 1588–1597.

Marin, O. (2012). Interneuron dysfunction in psychiatric disorders. Nat. Rev. Neurosci. *13*, 107–120.

Maroof, A.M., Keros, S., Tyson, J.A., Ying, S.W., Ganat, Y.M., Merkle, F.T., Liu, B., Goulburn, A., Stanley, E.G., Elefanty, A.G., et al. (2013). Directed differentiation and functional maturation of cortical interneurons from human embryonic stem cells. Cell Stem Cell *12*, 559–572.

Martinez-Cue, C., Delatour, B., and Potier, M.C. (2014). Treating enhanced GABAergic inhibition in Down syndrome: use of GABA alpha5-selective inverse agonists. Neurosci. Biobehav. Rev. *46*, 218–227.

Mayer, C., Hafemeister, C., Bandler, R.C., Machold, R., Batista Brito, R., Jaglin, X., Allaway, K., Butler, A., Fishell, G., and Satija, R. (2018). Developmental diversification of cortical inhibitory interneurons. Nature *555*, 457–462.

Mito, T., Pereyra, P.M., and Becker, L.E. (1991). Neuropathology in patients with congenital heart disease and Down syndrome. Pediatr. Pathol. *11*, 867–877.

Nicholas, C.R., Chen, J., Tang, Y., Southwell, D.G., Chalmers, N., Vogt, D., Arnold, C.M., Chen, Y.J.J., Stanley, E.G., Elefanty, A.G., et al. (2013). Functional Maturation of hPSC-derived forebrain interneurons Requires an extended Timeline and mimics human neural development. Cell Stem Cell *12*, 573–586.

Olmos-Serrano, J.L., Kang, H.J., Tyler, W.A., Silbereis, J.C., Cheng, F., Zhu, Y., Pletikos, M., Jankovic-Rapan, L., Cramer, N.P., Galdzicki, Z., et al. (2016). Down syndrome developmental brain transcriptome reveals defective oligodendrocyte Differentiation and myelination. Neuron *89*, 1208–1222.

Paredes, M.F., James, D., Gil-Perotin, S., Kim, H., Cotter, J.A., Ng, C., Sandoval, K., Rowitch, D.H., Xu, D., McQuillen, P.S., et al. (2016). Extensive migration of young neurons into the infant human frontal lobe. Science *354*, aaf7073.

Parnavelas, J.G., Anderson, S.A., Lavdas, A.A., Grigoriou, M., Pachnis, V., and Rubenstein, J.L. (2000). The contribution of the ganglionic eminence to the neuronal cell types of the cerebral cortex. Novartis. Found. Symp. *228*, 129–139. discussion 139-147.

Perl, D.P., Good, P.F., Bussiere, T., Morrison, J.H., Erwin, J.M., and Hof, P.R. (2000). Practical approaches to stereology in the setting of aging- and disease-related brain banks. J. Chem. Neuroanat. *20*, 7–19.

Pi, H.-J., Hangya, B., Kvitsiani, D., Sanders, J.I., Huang, Z.J., and Kepecs, A. (2013). Cortical interneurons that specialize in disinhibitory control. Nature *503*, 521–524.

Potier, M.C., Braudeau, J., Dauphinot, L., and Delatour, B. (2014). Reducing GABAergic inhibition restores cognitive functions in a mouse model of Down syndrome. CNS Neurol. Disord. Drug Targets *13*, 8–15.

Radonjic, N.V., Ayoub, A.E., Memi, F., Yu, X., Maroof, A., Jakovcevski, I., Anderson, S.A., Rakic, P., and Zecevic, N. (2014). Diversity of cortical interneurons in primates: the role of the dorsal proliferative niche. Cell Rep. *9*, 2139–2151.

Reinchisi, G., Ijichi, K., Glidden, N., Jakovcevski, I., and Zecevic, N. (2012). COUP-TFII expressing interneurons in human fetal forebrain. Cereb. Cortex *22*, 2820–2830.

Rong, X., Chen, C., Zhou, P., Zhou, Y., Li, Y., Lu, L., Liu, Y., Zhou, J., and Duan, C. (2014). R-spondin 3 regulates dorsoventral and anteroposterior patterning by antagonizing Wnt/β-catenin signaling in zebrafish embryos. PLoS One *9*, e99514.

Ross, M.H., Galaburda, A.M., and Kemper, T.L. (1984). Down's syndrome: is there a decreased population of neurons? Neurology *34*, 909–916.

Rossignol, E. (2011). Genetics and function of neocortical GABAergic interneurons in neurodevelopmental disorders. Neural. Plast. *2011*, 649325.

Schmidt-Sidor, B., Wisniewski, K.E., Shepard, T.H., and Sersen, E.A. (1990). Brain growth in Down syndrome subjects 15 to 22 weeks of gestational age and birth to 60 months. Clin. Neuropathol. *9*, 181–190.

Shi, Y., Wang, M., Mi, D., Lu, T., Wang, B., Dong, H., Zhong, S., Chen, Y., Sun, L., Zhou, X., et al. (2021). Mouse and human share conserved transcriptional programs for interneuron development. Science *374*, eabj6641.

Stagni, F., Giacomini, A., Emili, M., Guidi, S., and Bartesaghi, R. (2018). Neurogenesis impairment: An early developmental defect in Down syndrome. Free. Radic. Biol. Med. *114*, 15–32.

Takashima, S., Becker, L.E., Armstrong, D.L., and Chan, F. (1981). Abnormal neuronal development in the visual cortex of the human fetus and infant with down's syndrome. A quantitative and qualitative Golgi study. Brain Res. *225*, 1–21.

Weitzdoerfer, R., Dierssen, M., Fountoulakis, M., and Lubec, G. (2001). Fetal life in Down syndrome starts with normal neuronal density but impaired dendritic spines and synaptosomal structure. JNeural TransmSuppl *2001*, 59–70.

West, M.J. (2013). Optimizing the sampling scheme for a stereological study: how many individuals, sections, and probes should be used. Cold Spring Harb. Protoc. *2013*, 521–532.

West, M.J., Slomianka, L., and Gundersen, H.J. (1991). Unbiased stereological estimation of the total number of neurons in thesubdivisions of the rat hippocampus using the optical fractionator. Anat. Rec. *231*, 482–497.

Wilson, S.W., and Rubenstein, J.L. (2000). Induction and dorsoventral patterning of the telencephalon. Neuron *28*, 641–651.

Wisniewski, K.E. (1990). Down syndrome children often have brain with maturation delay, retardation of growth, and cortical dysgenesis. Am. J. Med. Genet. Suppl. *7*, 274–281.

Wisniewski, K.E., Laure-Kamionowska, M., and Wisniewski, H.M. (1984). Evidence of arrest of neurogenesis and synaptogenesis in brains of patients with Down's syndrome. N. Engl. J. Med. *311*, 1187–1188.

Xu, Q., Cobos, I., De La Cruz, E., Rubenstein, J.L., and Anderson, S.A. (2004). Origins of cortical interneuron subtypes. J. Neurosci. *24*, 2612–2622.

Xu, Q., Guo, L., Moore, H., Waclaw, R.R., Campbell, K., and Anderson, S.A. (2010). Sonic hedgehog signaling confers ventral telencephalic progenitors with distinct cortical interneuron fates. Neuron *65*, 328–340.

Xu, Q., Tam, M., and Anderson, S.A. (2008). Fate mapping Nkx2.1-lineage cells in the mouse telencephalon. J. Comp. Neurol. *506*, 16–29.

Xu, Q., Wonders, C.P., and Anderson, S.A. (2005). Sonic hedgehog maintains the identity of cortical interneuron progenitors in the ventral telencephalon. Development *132*, 4987–4998.

Xu, R., Brawner, A.T., Li, S., Liu, J.J., Kim, H., Xue, H., Pang, Z.P., Kim, W.Y., Hart, R.P., Liu, Y., and Jiang, P. (2019). OLIG2 drives abnormal neurodevelopmental Phenotypes in Human iPSC-based Organoid and chimeric mouse Models of down syndrome. Cell Stem Cell *24*, 908–926.e908.

Zhou, Y., Zhou, B., Pache, L., Chang, M., Khodabakhshi, A.H., Tanaseichuk, O., Benner, C., and Chanda, S.K. (2019). Metascape provides a biologist-oriented resource for the analysis of systems-level datasets. Nat. Commun. *10*, 1523.

Zorrilla de San Martin, J., Delabar, J.M., Bacci, A., and Potier, M.C. (2018). GABAergic over-inhibition, a promising hypothesis for cognitive deficits in Down syndrome. Free Radic. Biol. Med. *114*, 33–39.

Stem Cell Reports, Volume *17*

Supplemental Information

Altered patterning of trisomy 21 interneuron progenitors

Yathindar Giffin-Rao, Jie Sheng, Bennett Strand, Ke Xu, Leslie Huang, Margaret Medo, Kirstin A. Risgaard, Samuel Dantinne, Sruti Mohan, Aratrika Keshan, Roger A. Daley Jr., Bradley Levesque, Lindsey Amundson, Rebecca Reese, André M.M. Sousa, Yunlong Tao, Daifeng Wang, Su-Chun Zhang, and Anita Bhattacharyya

Figure S1, related to Figure 3

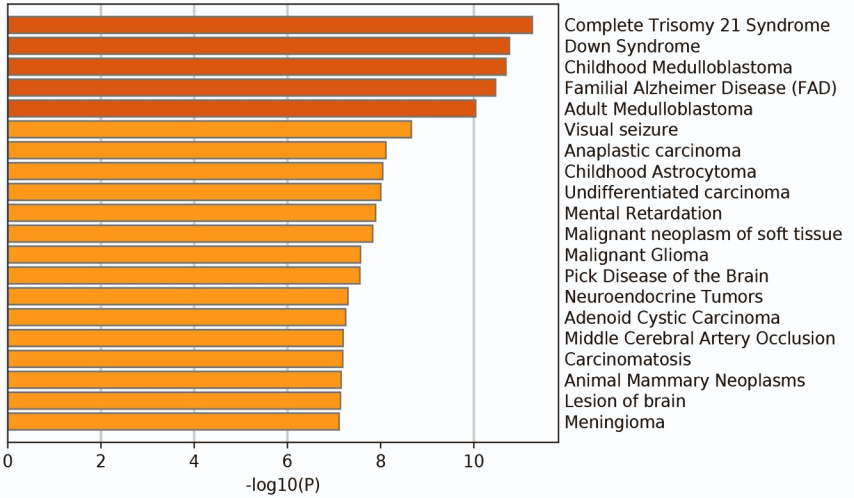

DEG pathways identified by DisGeNet database.

Figure S2, related to Figure 3

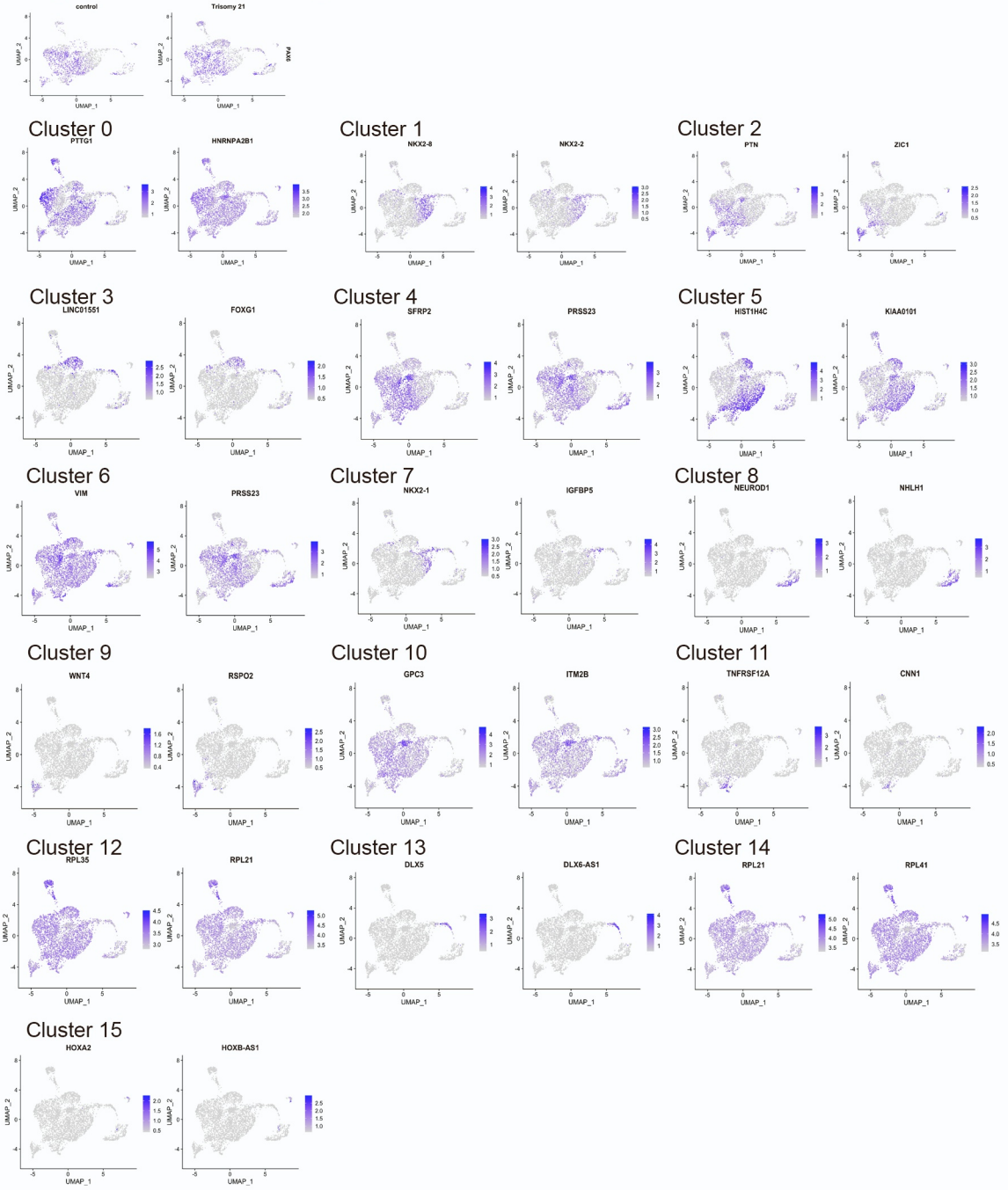

Figure S3, related to Figure 4

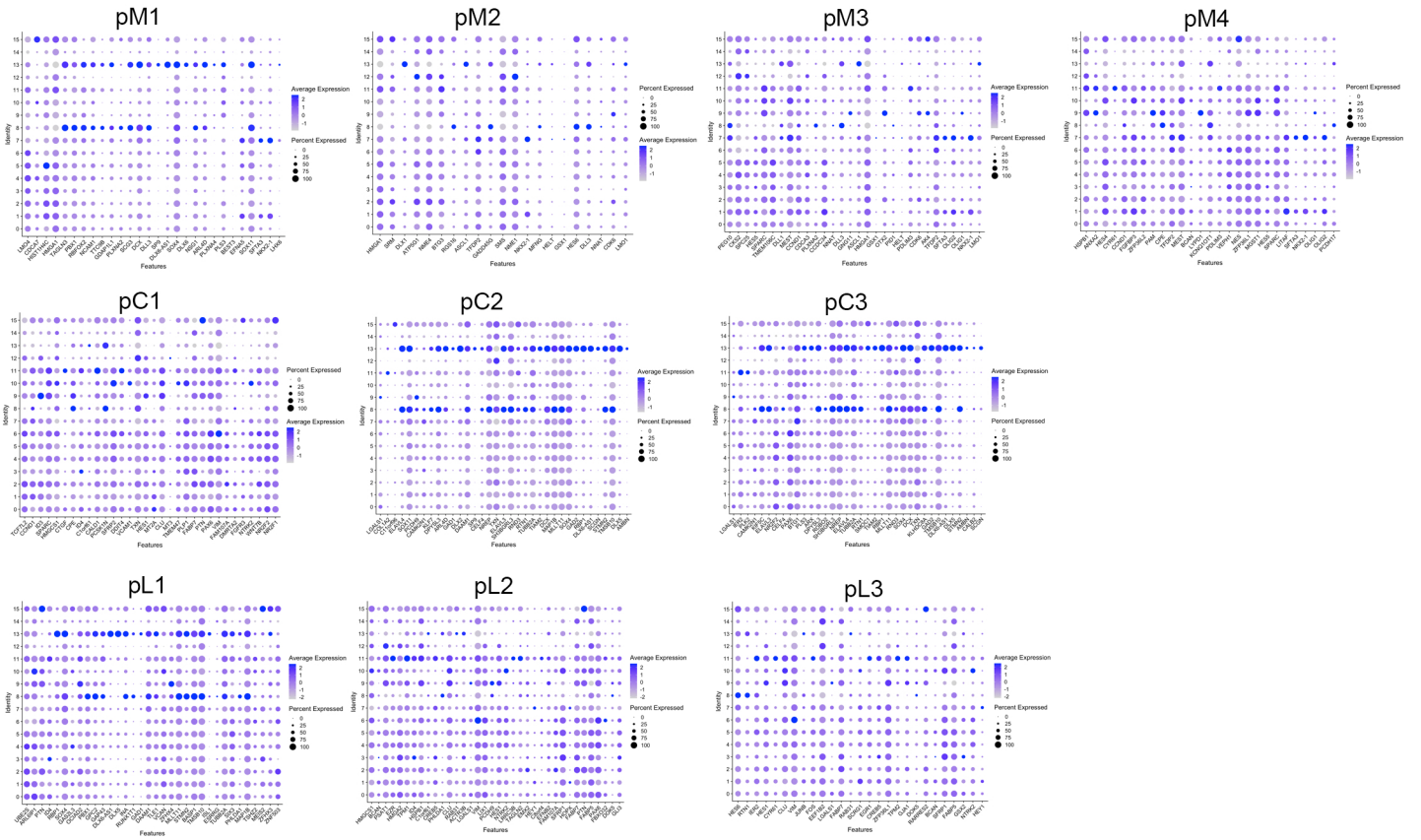

Dot plots comparing gene expression in iPSCs clusters (Figure 4) (y-axis) to gene expression in fetal ganglionic eminences subclusters (Shi et al., 2021) (x-axis).

Supplemental Experimental Procedures

Quantification of neurons in post-mortem brain

Tissue: Adult postmortem brain tissue was obtained from the NICHD Brain and Tissue Bank for Developmental Disorders with approval from the University of Wisconsin-Madison Institutional Review Board. Superior temporal gyrus or Brodmann's Area 22 was obtained from four DS individuals and age and gender matched control subjects. It should be noted that the post mortem interval (PMI) varied between the samples and, in particular, the DS samples had longer PMIs than their matched controls (Controls 14.50 ± 1.26, DS 25.00 ± 4.5, p=0.11 calculated using non-parametric Mann-Whitney U test).

Subject and sample information

UMB number	Diagnosis	Age (years, days)	Sex	Race	Post mortem interval (hours)
1841	Control	19, 289	Male	Caucasian	14
5277	Ts21	19, 352	Male	Caucasian	26
5654	Control	19, 264	Male	Caucasian	18
M1960M	Ts21	19, 311	Male	Caucasian	14
5030	Control	24, 333	Male	Afr Amer	14
5341	Ts21	25, 304	Male	Afr Amer	24
1544	Control	32, 315	Male	Caucasian	12
4273	Ts21	33, 315	Male	Caucasian	36

Immunocytochemistry: Tissues were sectioned at 50 microns using a cryostat and processed for immunocytochemistry. Antigen-antibodies were visualized with avidin-biotin, horseradish peroxidase (HRP) and 3, 3'-Diaminobenzidine (DAB) using standard immunohistochemical techniques on floating sections.

Immunocytochemical methods

MARKER		ANTIBODY INFORMATION	ANTIGEN RETRIEVAL	DILUTION	secondary, ABC	DAB
all neurons	NeuN	AbCam ab104225 Rabbit	Vector unmasking 15 minutes 95°C	1:500	Visucyte HRP polymer	5 minutes ImPACT
Parvalbumin	PV	Sigma P3088 mouse	Vector unmasking 5 minutes 95°C	1:1000	Biotin 2' ABC	5 minutes
Somatostatin	SST	Millipore MAB354 rat	Vector unmasking 15 minutes 95°C	1:100	Biotin 2' ABC	10 minutes
Calretinin	CR	Swant CR7697 Rabbit	Vector unmasking 15 minutes 95°C	1:2000	Biotin 2' ABC	3 minutes

Quantification of positive cells: Total numbers of NeuN+, PV+, CR+ and SST+ neurons were estimated using the Optical Fractionator (OF) workflow in Stereo Investigator software (MBF Bioscience). Six to eight sections at an interval of 5-7 were analyzed. Percentages of tissue for sampling were chosen based on the resample oversample function in Stereo Investigator (PV: 1%, CR: 1%) to ensure a coefficient of error < 0.1.The total positive cell count was estimated using the following equation: $N = \sum Q * \frac{t}{h} * \frac{1}{asf} * \frac{1}{ssf}$, where $\sum Q$is the total

number of cells counted, *t* the average section thickness and *h* the height of the optical dissector, and *asf* and *ssf* the area sectioning fraction and the section sampling fractions, respectively [10].

Volume and density calculation: Total volume of tissue sampled and counted was estimated using the Cavalieri Estimator probe (Stereo Investigator, MBF Bioscience). The total cell population estimate (from the Optical Fractionator Workflow) was divided by the total tissue volume (from the Cavalieri Estimator) to calculate cell density.

Human induced pluripotent stem cells (iPSCs)

iPSCs: We established one new isogenic Ts21 iPSC pair and additional iPSCs from DS individuals and unaffected controls (**Table S2**). Primary dermal fibroblasts were isolated from tissue acquired with approval from the University of Wisconsin-Madison Human Subjects Institutional Review Board (protocol #2016–0979). Fibroblasts were reprogrammed by electroporation delivery of episomal vectors pCXLE-hOCT3/4-shp53-F (Addgene, 27077), pCXLE-hSK (Addgene, 27078) and pCXLE-hUL (Addgene, 27080). After electroporation, cells were cultured on mouse embryonic fibroblast (MEF) feeder cells in a low oxygen incubator (5% O_2, 5% CO_2). Cells were fed with hESCM (DMEM-F12 media (Gibco) with 20% knock-out serum replacement (Gibco), 1X Non-Essential Amino Acids (Life Technologies), 0.5X GlutaMAX (Life Technologies), 0.1 mM 2-mercaptoethanol (Sigma), and 12 ng/mL bFGF (Waisman Biomanufacturing)). The iPSC colonies were manually picked between day 14–28 post-transfection. Following expansion, cells were transferred onto Matrigel (R&D) and cultured with mTeSR1 (Stemcell Technologies) for banking. iPSCs on MEF were passaged with dispase solution (Gibco) Split ratio is 1 to 6 every 5–7 days., and iPSCs on Matrigel were passaged with 0.5mM EDTA or ReLeSR (05872, Stemcell Technologies).

Cell line	Sex	Age (years)	Karyotype	Relationship	Reprogramming method
WC-24-B	Female	25	Normal	Isogenic pair	Episomal
WC-24-M			Trisomy 21		
DS2U	Male	1	Normal	Isogenic pair	Retroviral
DS1			Trisomy 21		
603-8	Male	36	Normal	Unrelated	Retroviral
WC-38-01	Male	35	Trisomy 21		Sendai
WC-58-07	Female	Neonate	Normal	Unrelated	Episomal
WC-20-02	Female	3	Trisomy 21		Episomal

Cell culture: iPSCs were maintained on MEFs in hESC media (DMEM/F-12/KOSR/L-Glut/MEM-NEAA/FGF-2) and passaged with collagenase. Differentiation to interneuron progenitors was carried out as described (Liu et al., 2013). When ~80% confluent, iPSCs were dissociated from MEFs using dispase to generate embryoid bodies (EBs). EBs were maintained in suspension with dual SMAD inhibition for 4 days and then media was changed to neural induction media (NIM; DME/F12 media with N2, NEAA and heparin). EBs were plated on Day 7 and SHH was added on Day 10. For neurons, EBs were lifted to neurospheres on Day 15 or 16 and maintained in NIM with B27 and purmorphamine. For neuronal differentiation, progenitors in neurospheres were dissociated with Accutase and plated on polyornithine/laminin-coated coverslips in neural differentiation medium containing DMEM/F12, N2(1:50), B27 (1:100), 10 ng/mL brain derived neurotrophic factor (BDNF) (Peprotech), 10 ng/mL glial derived neurotrophic factor(GDNF) (R&D Systems), cAMP (Sigma), and ascorbic acid(Sigma). Compound E (gamma secretase inhibitor XXI) was added at plating.

Cellular analysis

Cell proliferation: Cell proliferation was assayed using Click-iT™ EdU Alexa Fluor™ 488 Imaging Kit. A final concentration of 10uM EdU was added to cells for 8 hours. Cells were fixed with 4% paraformaldehyde in PBS

for 15 minutes and processed for immunofluorescence for phospho-histone H3 (pHH3, Cell Signaling Technology #9706).

Immunofluorescence: Neural progenitors in neurospheres were dissociated with Accutase and plated onto laminin coated 96 well cell culture plates or coverslips at 50-60,000 cells/well/coverslip. The day after plating, cells were fixed with 4% paraformaldehyde in PBS for 15 minutes. Cells were rinsed with PBS and incubated with a permeabilization/blocking buffer (5% normal goat serum, 0.1% TritonX-100 in PBS) for 30 minutes. Cells were incubated with primary antibodies to NKX2.1 and/or COUP-TFII overnight followed by fluorescent secondary antibodies, washed with PBS and mounted in Fluoromount.

Antigen	Company and catalog number
NKX2.1/TTF1	abCAM ab76013
COUP-TFII/NRF2	R&D systems PP-H7147-00
Calretinin	Swant 7697
Somatostatin	Millipore MAB354
Phospho-Histone H3 (Ser10)	Cell Signaling Technology 9706

High Content Imaging analysis: Imaging and analysis was done using the high content imager Operetta (Perkin Elmer) at 20x magnification.

Molecular analysis

qPCR: RNA was isolated from progenitors using the ZYMO Research Direct-Zol RNA Miniprep plus kit followed by cDNA synthesis using qScript cDNA Supermix. qPCR was done in triplicate on 2-3 batches of differentiation (N=3). Data are presented as Fold Change calculated from ddCt values. Error bars indicate fold change of ddCt values +/- 1 SD. Statistical significance was determined by one-sample t-test on ddCt values.

Gene	Forward Seq (5' – 3')	Reverse Seq (5' – 3')
AXIN2	TATCCAGTGATGCGCTGA	CGGTGGGTTCTCGGGAAATG
NR2F2/COUPTFII	CTCAAGGCCATAGTCCTGTCC	GGTACTGGCTCCTAACGTATTC
FZD1	ATCTTCTTGTCCGGCTGTTACA	GTCCTCGGCGAACTTGTCATT
GLI1	AACGCTATACAGATCCTAGCTCG	GTGCCGTTTGGTCACATGG
GLI2	CCCCTACCGATTGACATGCG	GAAAGCCGGATCAAGGAGATG
GLI3	GAAGTGCTCCACTCGAACAGA	GTGGCTGCATAGTGATTGCG
LEF1	ATGTCAACTCCAAACAAGGCA	CCCGGAGACAAGGGATAAAAAGT
LRP5	CGACACTGGGACCAACAGAA	AGATGTAGCCCTTGGTGGGA
LRP6	CTGAGAGCGGCCCCTTTGTT	GCATCCTCCAAGCCTCCAAC
NKX 2.1	AGCACACGACTCCGTTCTC	GCCCACTTTCTTGTAGCTTTCC
PTCH1	GGAGCAGATTTCCAAGGGGA	CCACAACCAAGAACTTGCCG
PTCH2	CCGCCAGAGGTGATACAGAT	CCACGGTCATGGAGGTAGTC
SMO	ACTTGGATTGCGAGGCTAGG	TCGCAAACTTTGGAACCCG

Quantification and Statistical Analysis

All experiments include at least three biological replicates (batches of differentiation, N=3 or individual cell lines N=4) and 3 technical replicates (n=3) for each cell line. Ts21 and control pairs were differentiated together. Data were analyzed using GraphPad Prism version 8. All pooled data are presented as mean ± standard error of the mean (SEM). Details regarding number of technical and biological replicates are provided in the figure legends with specific statistical analysis test used. For parametric datasets, data were analyzed using unpaired two-tailed

Student's t-test. For non-parametric datasets, an unpaired Mann-Whitney test was performed. ANOVA analyses were used for datasets with more than two groups. Kruskal-Wallis analysis of variance, one-way ANOVA followed by Dunn's post hoc or Dunnett's post hoc analysis or two-way ANOVA followed by post hoc Sidak's test or Tukey's test (GraphPad Prism 8). Differences were considered statistically significant at $p<0.05$.

Single Cell RNA sequencing analysis:

See R notebook

R Notebook

1 Prepare dataset

Load dataset. There are $4,292$ single cells and $33,694$ genes. The dataset contains two experimental groups:

- Control: 2,134 cells.
- Trisomy 21: 2158 cells.

```
library(dplyr)
library(Seurat)
library(patchwork)

rm(list=ls())
setwd("~/Desktop/Waisman/Anita/filtered_gene_bc_matrices_mex/GRCh38/")
mat = read.csv("./data.csv",header = FALSE)
features = read.table("./genes.tsv",sep='\t')
barcodes = read.table("./barcodes.tsv",sep='\t')
group = read.csv('./group.csv',row.names = 1)
colnames(mat) = features$V2
rownames(mat) = barcodes$V1

seuobj = CreateSeuratObject(t(mat),min.cells = 0)
seuobj <- AddMetaData(object = seuobj, metadata = group, col.name = 'group')
```

2 QC and selecting cells for further analysis

The three QC metrics shown in the following violin figures are:

- The number of unique genes detected in each cell:
    - Low-quality cells or empty droplets will often have very few genes;
    - Cell doublets or multiplets may exhibit an aberrantly high gene count.
- The total number of molecules detected within a cell.
- The percentage of reads that map to the mitochondrial genome:
    - Low-quality / dying cells often exhibit extensive mitochondrial contamination.

```
seuobj[["percent.mt"]] <- PercentageFeatureSet(seuobj, pattern = "^MT-")
VlnPlot(seuobj, features = c("nFeature_RNA", "nCount_RNA", "percent.mt"), ncol = 3)
```

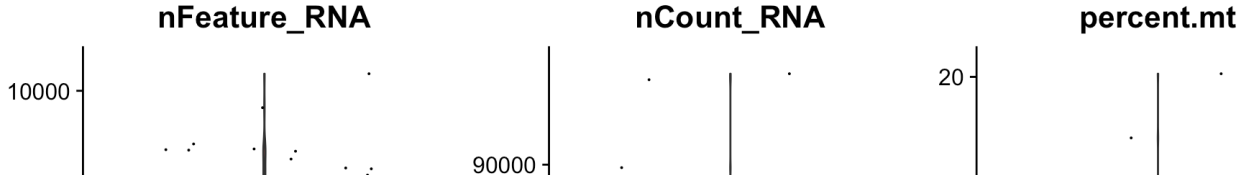

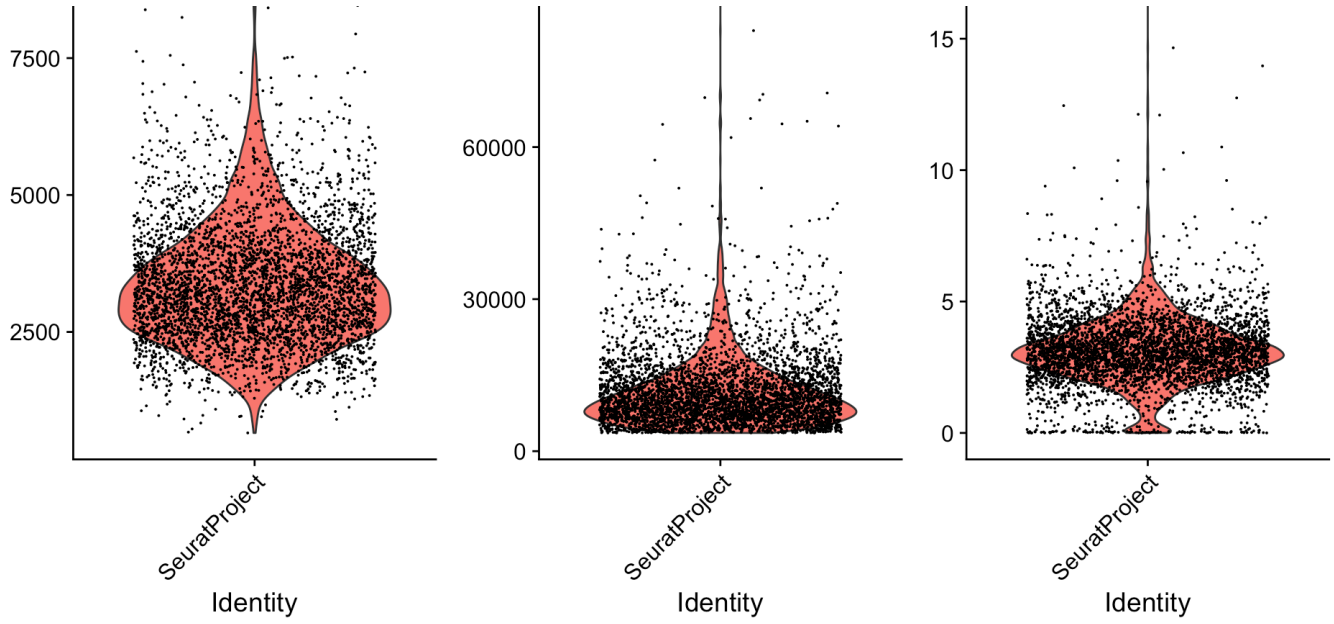

Filter cells that have detected unique genes less than 20 or over 10^5; filter cells that have $> 5\%$ mitochondrial counts. After filtering, the dataset remains $4,025$ cells (control: $2,003$; Trisomy 21: $2,022$).

```
seuobj <- subset(seuobj, subset = nFeature_RNA > 20 & nFeature_RNA < 10000 & percent.
mt < 5)
```

3 Perform integration

The joint analysis of two or more single-cell datasets might be problematic, especially identifying cell populations. We implement integrated analysis across different datasets to correct for technical differences between datasets (i.e., batch effect correction) and perform comparative scRNA-seq analysis across experimental conditions. First, we show the UMAP of all cells before integration, colored by experimental groups:

UMAP (Dataset before integrating)

```
seuobj <- NormalizeData(seuobj, verbose = FALSE)
seuobj <- FindVariableFeatures(seuobj, selection.method = "vst", nfeatures = 2000, ve
rbose = FALSE)
seuobj <- ScaleData(seuobj, verbose = FALSE)
seuobj <- RunPCA(seuobj, features = VariableFeatures(seuobj), verbose = FALSE)
seuobj <- RunUMAP(seuobj, reduction = "pca", dims = 1:30, verbose=FALSE)
DimPlot(seuobj, group.by = "group")
```

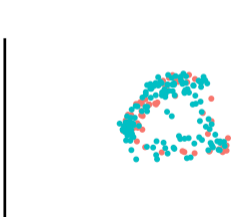

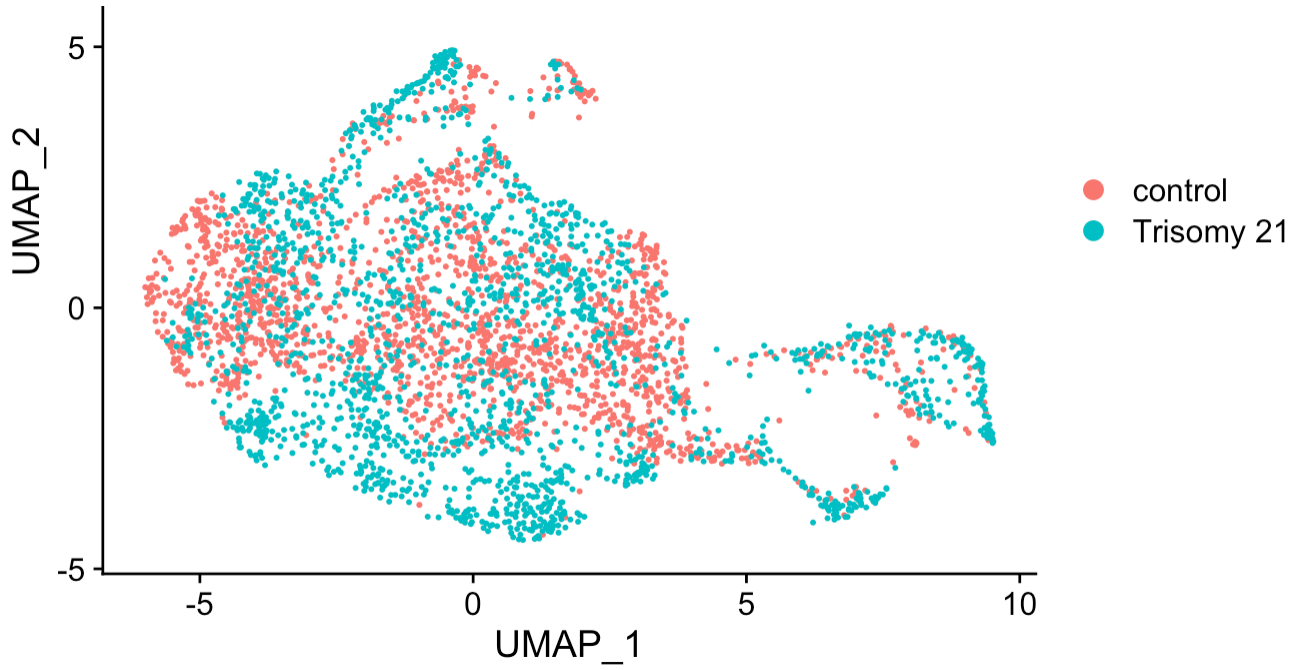

Integration

```
seuobj.list <- SplitObject(seuobj, split.by = "group")
seuobj.list <- lapply(X = seuobj.list, FUN = function(x) {
  x <- NormalizeData(x, verbose = FALSE)
  x <- FindVariableFeatures(x, selection.method = "vst", nfeatures = 2000, verbose =
FALSE)
})
features <- SelectIntegrationFeatures(object.list = seuobj.list)
seuobj.list <- lapply(X = seuobj.list, FUN = function(x) {
  x <- ScaleData(x, features = features, verbose = FALSE)
  x <- RunPCA(x, features = features, verbose = FALSE)
})
anchors <- FindIntegrationAnchors(object.list = seuobj.list, anchor.features = featur
es, verbose = FALSE)
combined <- IntegrateData(anchorset = anchors, verbose = FALSE)
DefaultAssay(combined) <- "integrated"
combined <- ScaleData(combined, verbose = FALSE)
```

Then, the following plot shows the UMAP of all cells after integration, colored by experimental groups:

UMAP (Dataset after integrating)

```
combined <- RunPCA(combined, features = VariableFeatures(combined),verbose = FALSE)
combined <- RunUMAP(combined, reduction = "pca", dims = 1:30, verbose=FALSE)
DimPlot(combined, group.by = "group")
```

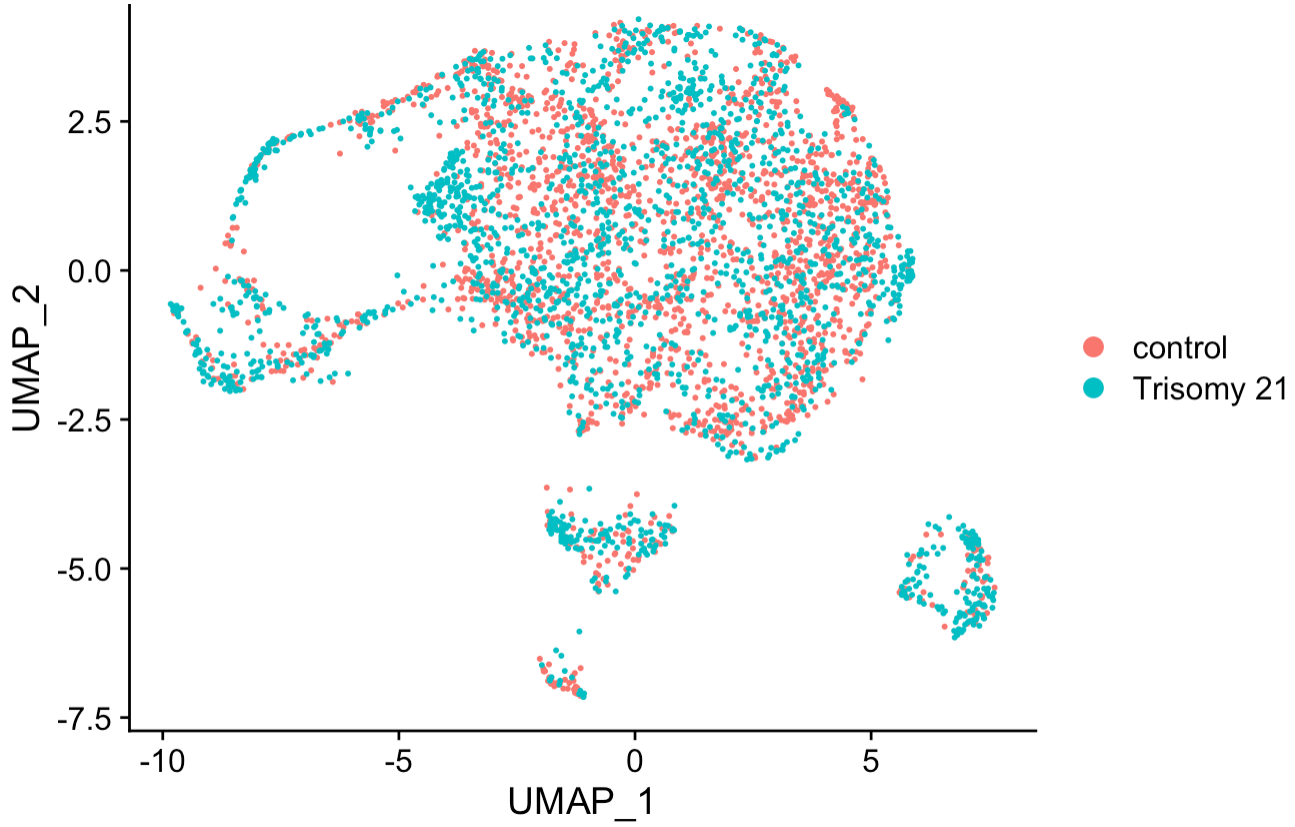

4 Regress out cell cycle genes

Then we mitigate the effects of cell cycle heterogeneity in the dataset by calculating cell cycle phase scores based on canonical markers, and regressing these out of the data during pre-processing.

Before cell cycle

Running a PCA on cell cycle genes reveals that cells separate entirely by phase.

```
s.genes <- cc.genes$s.genes
g2m.genes <- cc.genes$g2m.genes
combined <- CellCycleScoring(combined, s.features = s.genes, g2m.features = g2m.gene
s, set.ident = TRUE, verbose = FALSE)
combined <- RunPCA(combined, features = c(s.genes, g2m.genes), verbose = FALSE)
p1=DimPlot(combined,reduction="pca")
p2=DimPlot(combined,reduction="pca",group.by = "group")
p1+p2
```

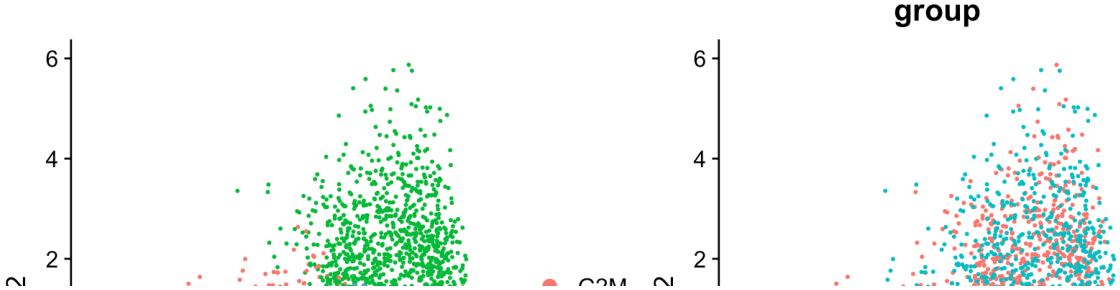

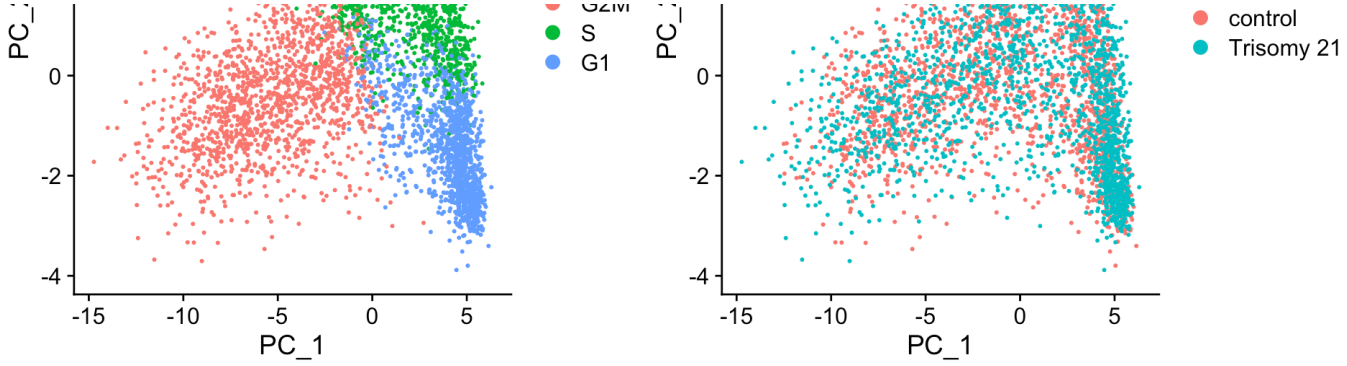

After cell cyle

When running a PCA on only cell cycle genes, cells no longer separate by cell-cycle phase.

```
combined <- ScaleData(combined, vars.to.regress = c("S.Score", "G2M.Score"), features
= rownames(combined), verbose=FALSE)
combined <- RunPCA(combined, features = c(s.genes, g2m.genes),verbose = FALSE)
DimPlot(combined, reduction="pca")
```

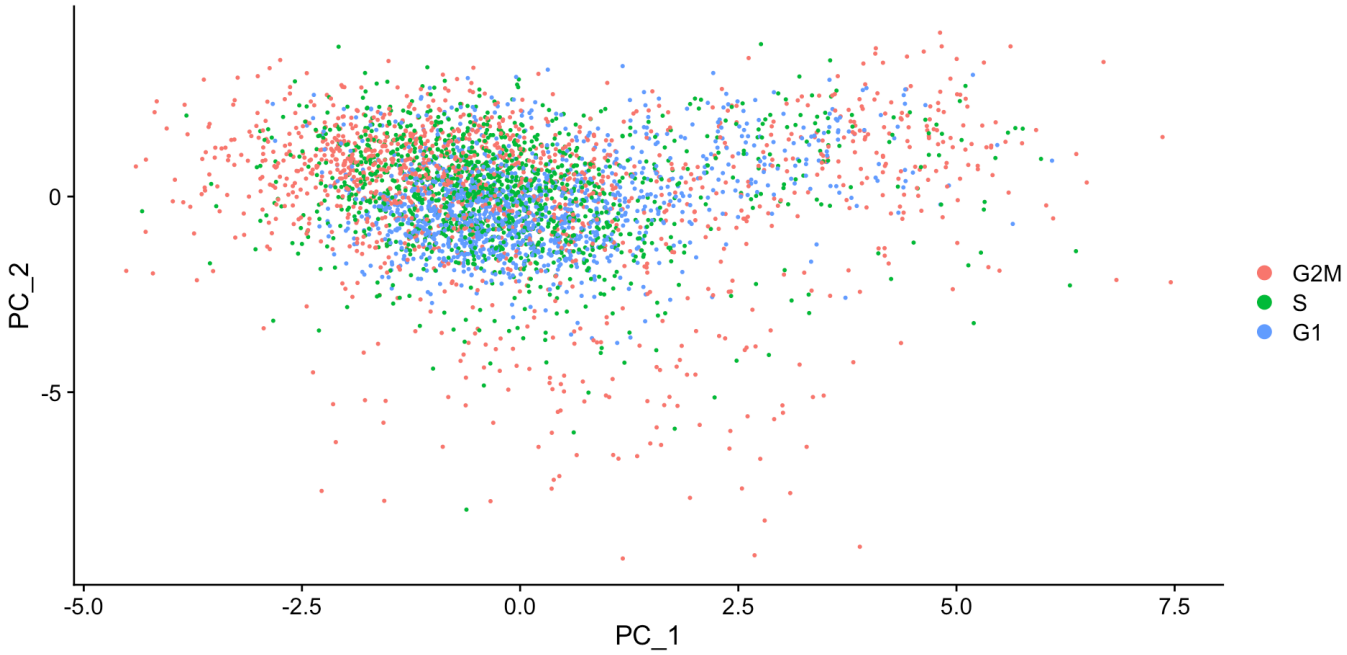


```
p1=DimPlot(combined,reduction="pca")
p2=DimPlot(combined,reduction="pca",group.by = "group")
p1+p2
```

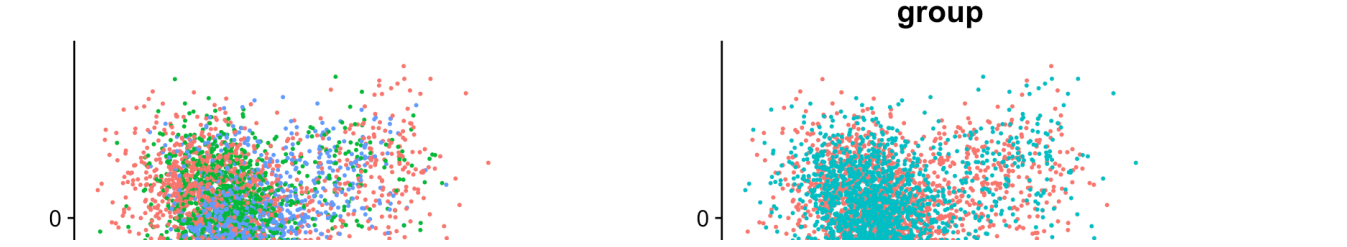

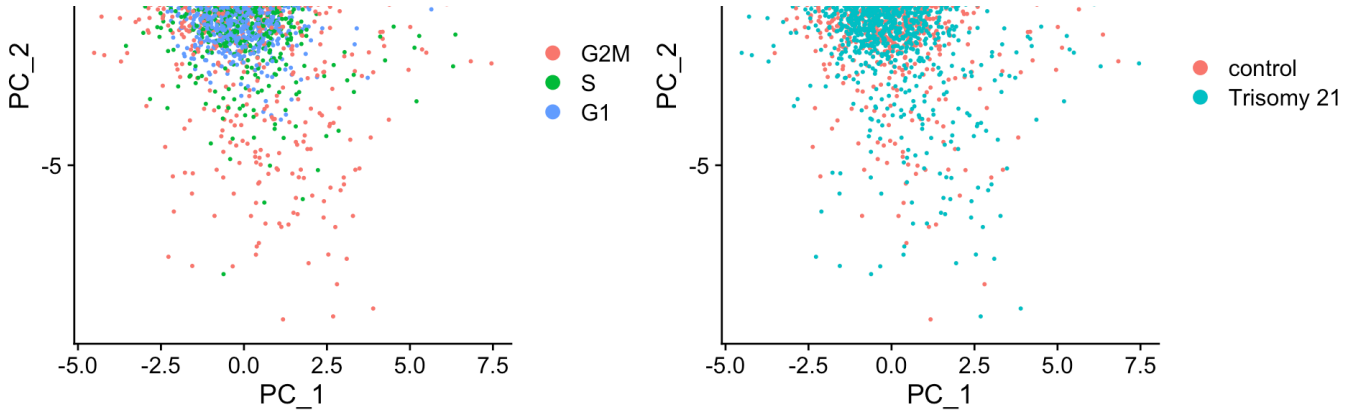

5 Dimensional reduction and clustering

Next, we perform PCA on the scaled data. By default, only the previously determined variable features are used as input. Then we visualize the dataset using UMAP after integration and mitigating cell cycle effects:

```
combined <- RunPCA(combined, features = VariableFeatures(combined), verbose = FALSE)
combined <- RunUMAP(combined, reduction = "pca", dims = 1:50, verbose = FALSE)
DimPlot(combined,pt.size = 0.3, group.by = "group")
```

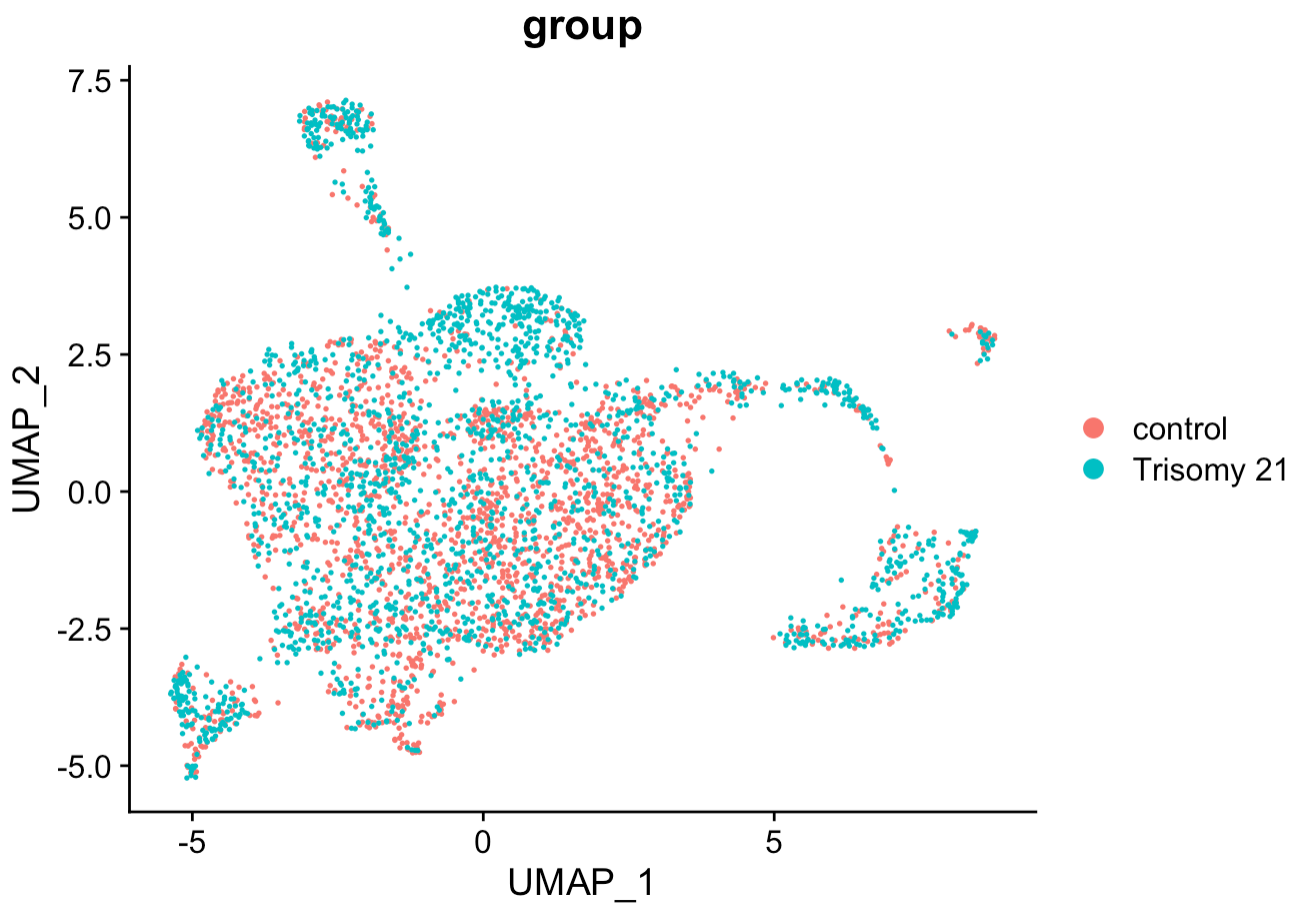

5.1 Cluster the cells

Visualize by experimental groups (left) and clustering results (right):

```
combined <- FindNeighbors(combined, reduction = "pca", dims = 1:50, verbose = FALSE)
combined <- FindClusters(combined, resolution = 1, verbose = FALSE)
p1 <- DimPlot(combined, pt.size = 0.3, reduction = "umap", group.by = "group")
p2 <- DimPlot(combined, pt.size = 0.3, reduction = "umap", label = TRUE, repel = TRU
E)
p1 + p2
```

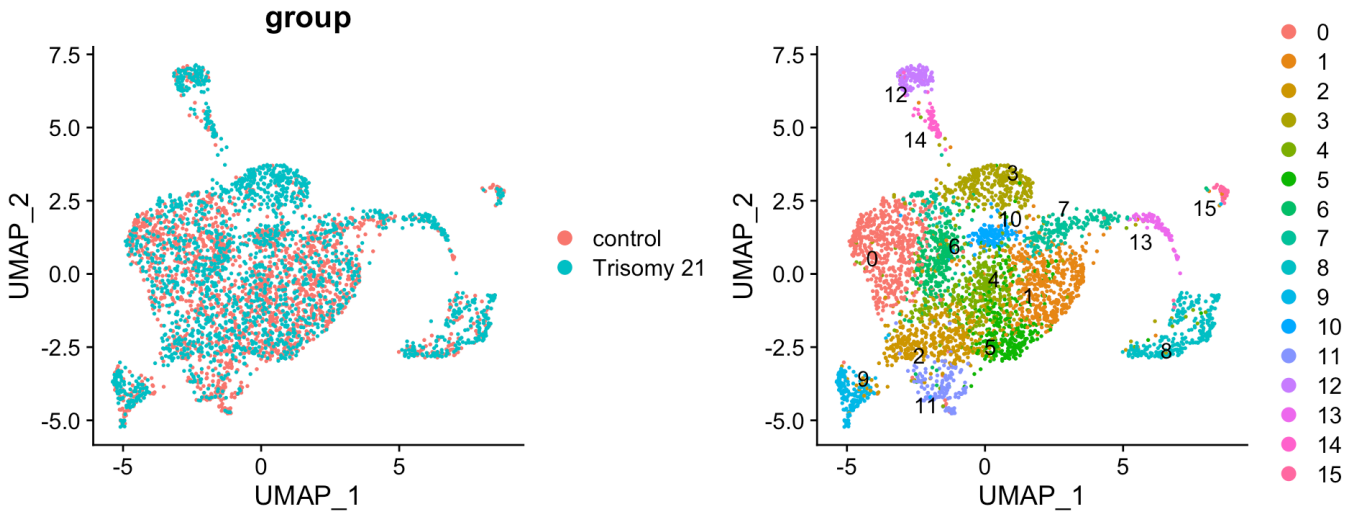

Visualize the two experimental conditions side-by-side (left: control; right: Trisomy 21):

```
DimPlot(combined, reduction = "umap", split.by = "group", label = TRUE, repel = TRUE)
```

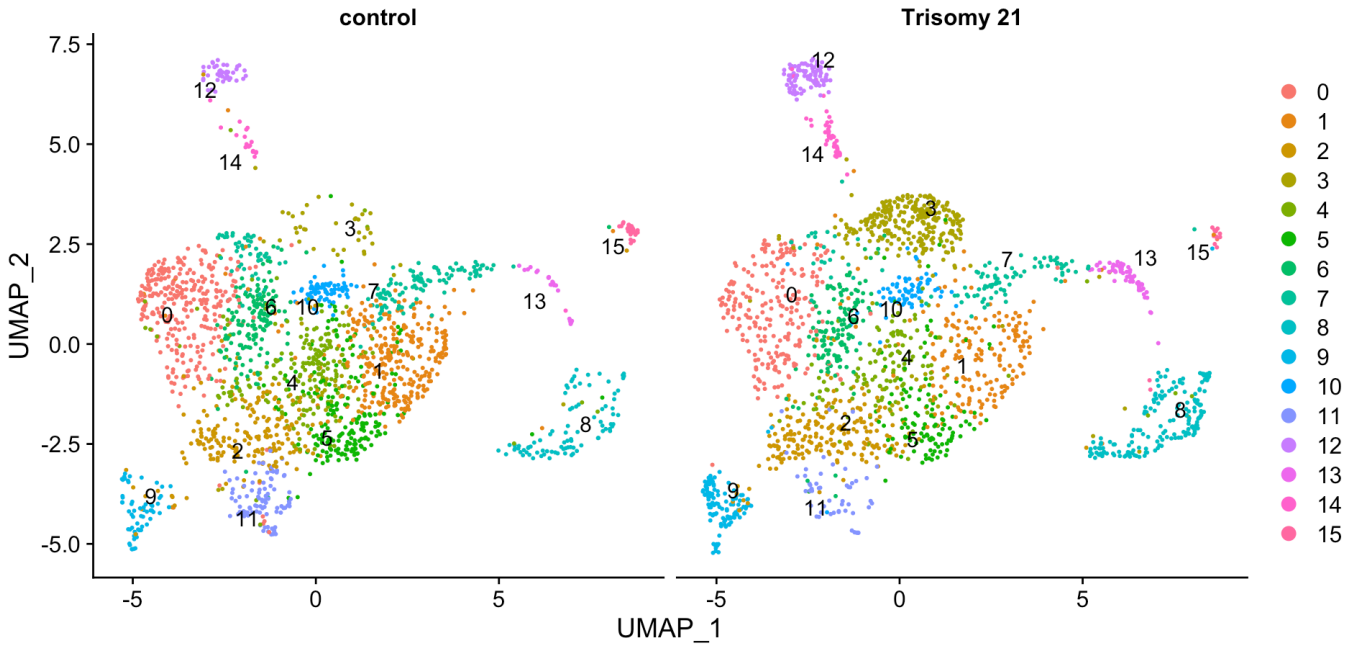

Check the number of cells in each cluster:

```
ncontrol=table(combined@meta.data[["seurat_clusters"]],combined@meta.data[["grou
p"]])[,1]
nTrisomy21=table(combined@meta.data[["seurat_clusters"]],combined@meta.data[["grou
p"]])[,2]
data.frame(`control`=ncontrol, `Trisomy 21`=nTrisomy21)
```

	control <int>	Trisomy.21 <int>
0	289	223
1	312	187
2	208	210
3	54	289
4	201	130
5	194	120
6	157	139
7	163	106
8	90	175
9	60	115

Check the percentage of cells in each cluster:

```
ncontrol=table(combined@meta.data[["seurat_clusters"]],combined@meta.data[["grou
p"]])[,1]
nTrisomy21=table(combined@meta.data[["seurat_clusters"]],combined@meta.data[["grou
p"]])[,2]
data.frame(`control (%)`=ncontrol/(ncontrol+nTrisomy21)*100, `Trisomy 21 (%)`=nTrisom
y21/(ncontrol+nTrisomy21)*100)
```

	control.... <dbl>	Trisomy.21.... <dbl>
0	56.44531	43.55469
1	62.52505	37.47495
2	49.76077	50.23923
3	15.74344	84.25656
4	60.72508	39.27492
5	61.78344	38.21656

	control.... <dbl>	Trisomy.21.... <dbl>
6	53.04054	46.95946
7	60.59480	39.40520
8	33.96226	66.03774
9	34.28571	65.71429

1-10 of 16 rows Previous **1** 2 Next

```
barplot(t(table(combined@meta.data[["seurat_clusters"]],combined@meta.data[["grou
p"]])), beside = TRUE, legend = TRUE)
```

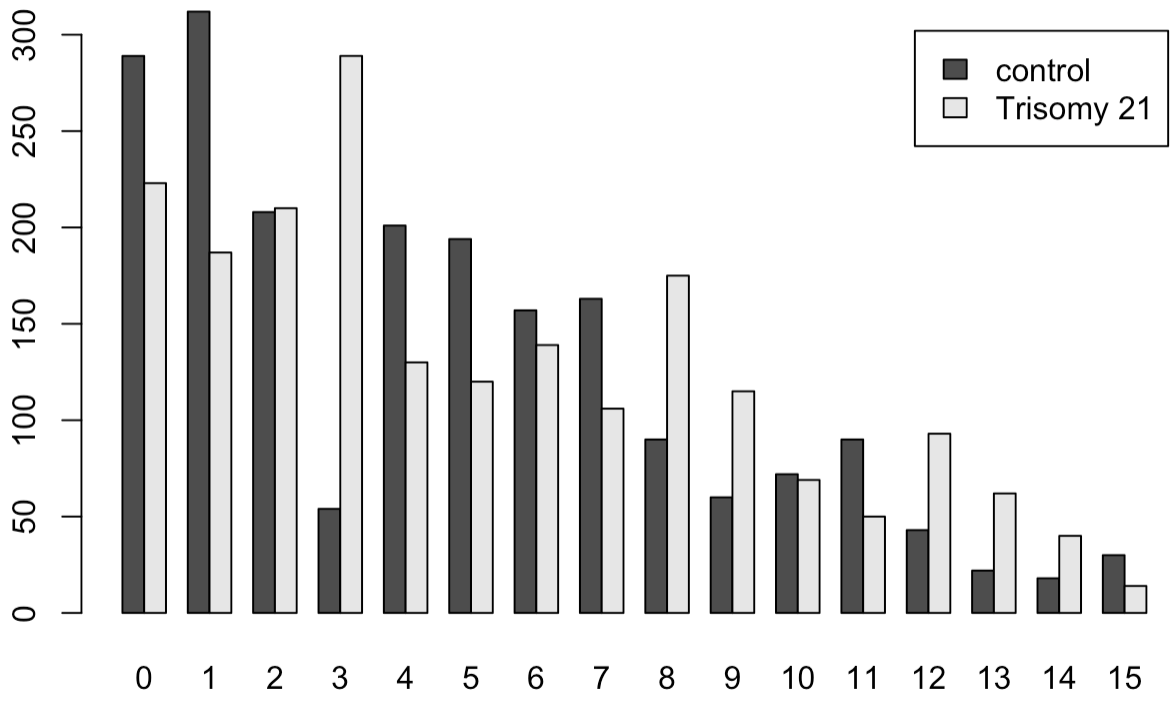

5.2 Fisher's exact test

We use Fisher's exact test to see whether the odds $\frac{\text{trisomy 21 cells in cluster 3}}{\text{trisomy 21 cells in cluster 1}} / \frac{\text{control group cells in cluster 3}}{\text{control group cells in cluster 1}}$ is greater than 1.

```
Testing = matrix(c(312,54,187,289),
                 nrow=2,
                 byrow=TRUE,
                 dimnames = list(Group = c("Control","Trisomy21"),
                                 Cluster = c("Cluster 1","Cluster 3")))
fisher.test(Testing, alternative = "greater")
```

```
##
##  Fisher's Exact Test for Count Data
##
## data:  Testing
## p-value < 2.2e-16
## alternative hypothesis: true odds ratio is greater than 1
## 95 percent confidence interval:
##  6.608068      Inf
## sample estimates:
## odds ratio
##    8.90362
```

Since p-value $< 2.2e^{-16} < 0.05$, under 95% confidence level, the odds $\frac{\text{trisomy 21 cells in cluster 3}}{\text{trisomy 21 cells in cluster 1}} / \frac{\text{control group cells in cluster 3}}{\text{control group cells in cluster 1}}$ is significantly greater than 1.

6 Detect differentially expressed genes (Positive markers only) for each cluster

6.1 Detect differentially expressed genes

Identify canonical cell type marker genes that are conserved across conditions. We perform differential gene expression testing for each group and combines the p-values using meta-analysis methods from the `MetaDE` R package. We identify differentially expressed genes in each cluster by choosing genes that combined p-values are less than 0.05.

```
DefaultAssay(combined) <- "RNA"
markers=list()
top5 = c()
for(i in 0:15){
  name <- paste('cluster', i,sep='')
  markers[[name]] <- FindConservedMarkers(combined, ident.1 = i, grouping.var = "grou
p", only.pos = TRUE, verbose = FALSE)
  markers[[name]] <- markers[[name]][(markers[[name]]$max_pval<0.05 &  markers[[nam
e]]$minimump_p_val<0.05),]
  top5=c(top5,rownames(markers[[i+1]])[1:5])
}
```

6.2 Feature plot of PAX6

Finally, we visualize the expression of PAX6 which might be of interest.

```
FeaturePlot(combined, pt.size = 0.3, features = "PAX6", min.cutoff = "q9", split.by = "group")
```

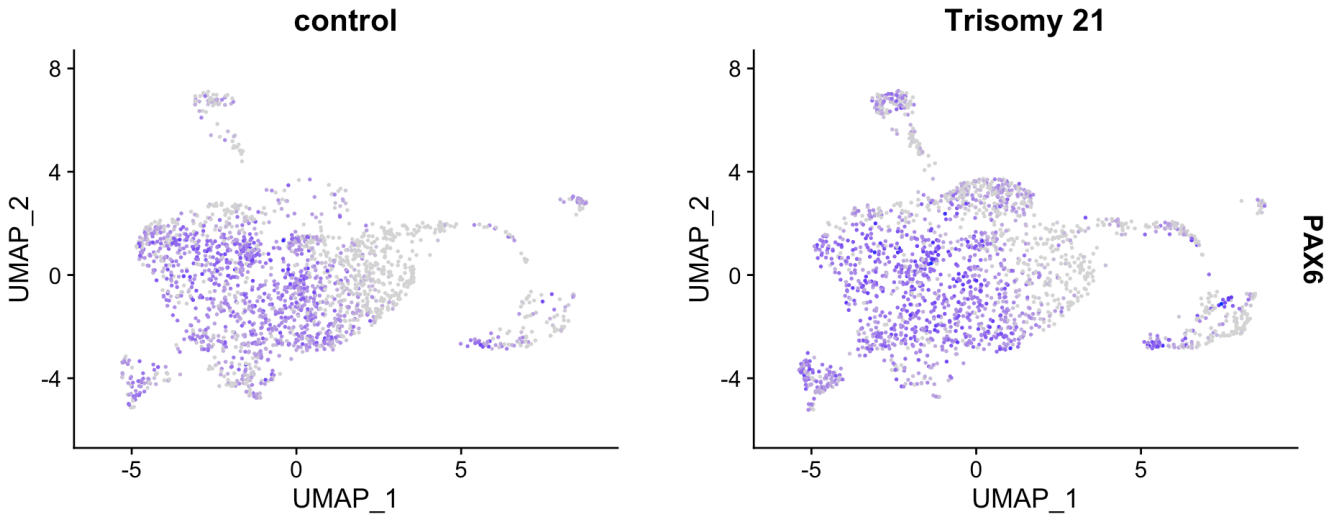

6.3 Additional feature plots

```
FeaturePlot(combined, pt.size = 0.3, features = c("NR2F2","GLI3","NNAT"), min.cutoff = "q8", split.by = "group")
```

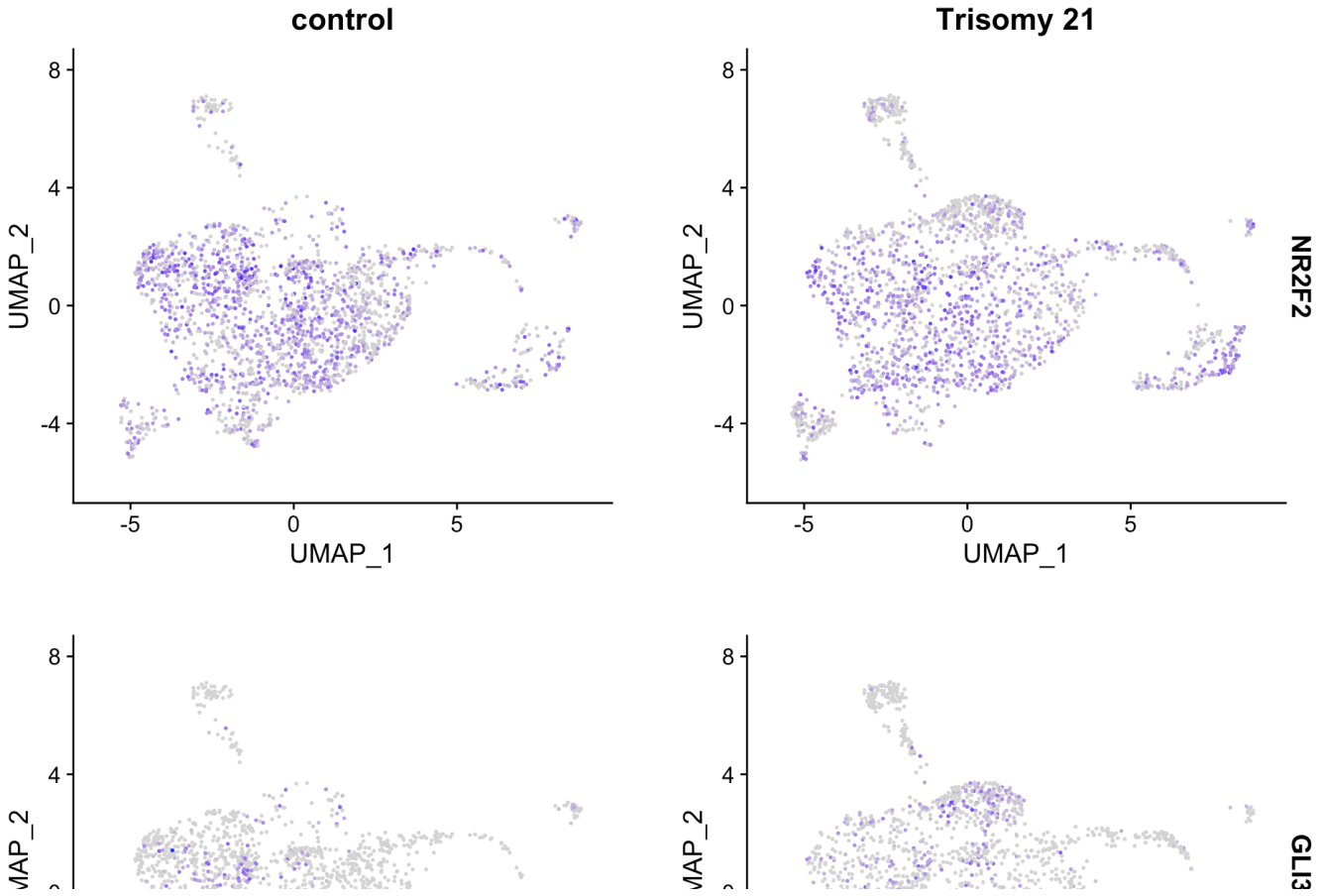

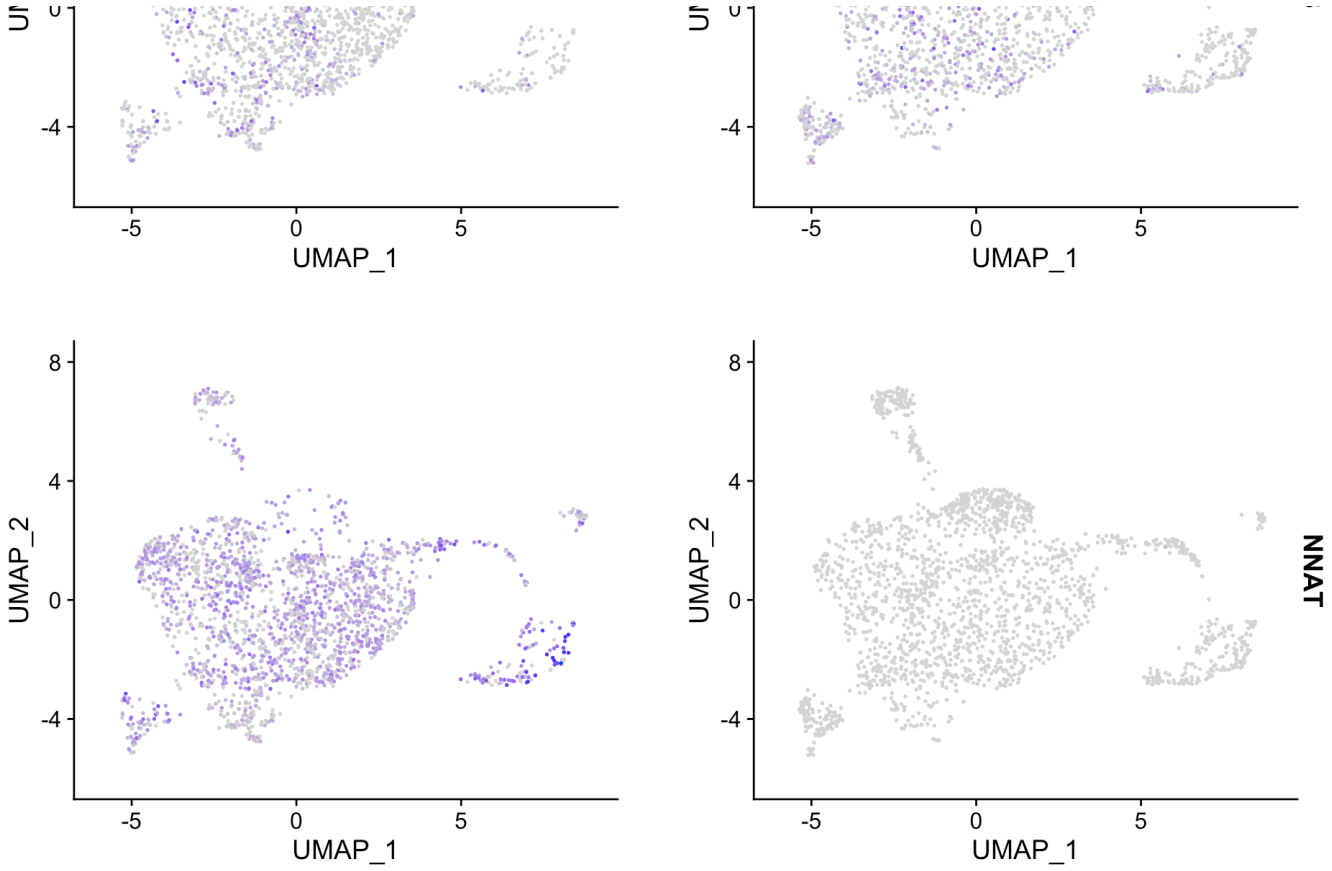

7 Detect differentially expressed genes for control vs Trisomy 21

```
dex_genes = FindMarkers(combined,group.by = "group", ident.1 = "control",verbose = FA
LSE)
dex_genes[dex_genes$p_val_adj<0.05,]
```

	p_val <dbl>	avg_log2FC <dbl>	pct.1 <dbl>	pct.2 <dbl>	p_val_adj <dbl>
NNAT	0.000000e+00	3.0307762	0.799	0.001	0.000000e+00
METRN	1.697330e-232	-0.9467797	0.575	0.865	5.718984e-228
MAGEH1	8.006321e-230	0.6742327	0.455	0.018	2.697650e-225
ATP5O	5.622243e-228	-0.6577688	0.966	0.996	1.894359e-223
POU3F4	6.785462e-226	0.8315352	0.471	0.033	2.286294e-221
SOD1	5.711082e-218	-0.7263670	0.946	0.987	1.924292e-213
PCSK1N	2.169855e-188	-1.0027290	0.058	0.469	7.311109e-184
TTC3	3.657587e-150	-0.6901749	0.827	0.941	1.232387e-145

	p_val	avg_log2FC	pct.1	pct.2	p_val_adj
	<dbl>	<dbl>	<dbl>	<dbl>	<dbl>
FGFBP3	1.053632e-147	1.1088862	0.928	0.769	3.550106e-143
TMSB4X	5.910802e-137	0.6586441	1.000	1.000	1.991586e-132